National Physical Laboratory

NPL REPORT IR 67

# CHANGES TO THE NPL REFERENCE AIR KERMA RATE PRIMARY STANDARD TH100C FOR HIGH DOSE RATE $^{192}$IR BRACHYTHERAPY SOURCES

T SANDER, I BILLAS, M KELLY, D J MAUGHAN, D R SHIPLEY

SEPTEMBER 2024

# Changes to the NPL reference air kerma rate primary standard TH100C for high dose rate $^{192}$Ir brachytherapy sources

T Sander, I Billas, M Kelly, D J Maughan, D R Shipley
Medical, Marine and Nuclear Department

## ABSTRACT

The NPL reference air kerma rate (RAKR) primary standard cavity ionisation chamber for high dose rate (HDR) $^{192}$Ir brachytherapy sources, designated as TH100C, was originally established in 2004. From 2004 to 2013, the cavity chamber was used to measure the RAKR of Nucletron microSelectron-v1 classic HDR $^{192}$Ir sources. This type of source became obsolete at the end of 2013. Since 2014, the cavity chamber has been used for measuring Elekta HDR $^{192}$Ir Flexisources instead. Switching from one source type to another required a re-evaluation of some of the primary standard conversion and correction factors in 2014. Additionally, the implementation of new physical data from ICRU report 90 required a recalculation of some of the Monte Carlo (MC) calculated correction factors. Pre-July 2019 calibrations for HDR $^{192}$Ir at NPL were based on data from ICRU report 37.

This NPL report is an update to NPL report DQL-RD 004 (Sander and Nutbrown 2006) and summarises the changes made to various primary standard correction factors since 2006. An updated uncertainty budget for the measurement of RAKR of an Elekta HDR $^{192}$Ir Flexisource and the calibration of secondary standard ionisation chambers is also presented.

ISSN 1754-2952

https://doi.org/10.47120/npl.IR67

National Physical Laboratory
Hampton Road, Teddington, Middlesex, TW11 0LW

This work was funded by the UK Government's Department for Science, Innovation & Technology through the UK's National Measurement System programmes.



Approved on behalf of NPLML by
Russell A S Thomas, Science Area Leader.

# CONTENTS

# 1 BACKGROUND

The National Physical Laboratory (NPL) has established a spherical graphite-walled cavity ionisation chamber (serial number TH100C) as the UK national air kerma primary standard for the measurement of the reference air kerma rate (RAKR) of high dose rate (HDR) $^{192}$Ir brachytherapy sources. The primary standard was originally established in 2004 to measure the RAKR of Nucletron microSelectron-v1 classic HDR $^{192}$Ir sources (model designation: 096.001). This type of radiation source became obsolete at the end of 2013. Since 2014, the cavity chamber has been used for measuring the RAKR of Elekta HDR $^{192}$Ir Flexisources (model designation: 136.147).

The first report on the HDR $^{192}$Ir primary standard, NPL report DQL-RD 004 (Sander and Nutbrown 2006), summarises the correction factors applicable to the cavity chamber response to realise RAKR of a Nucletron microSelectron-v1 classic HDR $^{192}$Ir source from first principles and to calibrate HDR brachytherapy secondary standard ionisation chambers. NPL report DQL-RD 004 also gives a detailed description of the cavity chamber and the associated measurement setup, including a lead collimator for the HDR $^{192}$Ir source which is still in use, i.e. these parts of the old report are still applicable to the current primary standard setup.

Changing the HDR $^{192}$Ir source type at NPL in 2014 required a revision of some of the primary standard correction factors.

Following the recommendations of the International Commission for Radiation Measurements and Units (ICRU) report 90 (ICRU 2016), certain conversion and correction factors pertinent to the standard required another re-evaluation in 2019.

ICRU report 90 recommends that the standard uncertainty of the value for $W_{air}$ is increased from previously 0.15% to now 0.35%. This change is reflected in the uncertainty analysis presented here.

This updated NPL report focuses on the description of the revised correction factors for the cavity chamber determined by either measurement or Monte Carlo (MC) simulations.

An updated uncertainty budget for the measurement of the RAKR of an Elekta HDR $^{192}$Ir Flexisource and the calibration of secondary standard ionisation chambers is also presented in this new report.

## 1.1 MAY 2004 – APRIL 2006

At the beginning of 2004, before the launch of NPL's HDR $^{192}$Ir brachytherapy calibration service, the first set of conversion and correction factors for cavity chamber TH100C and the RAKR measurement setup was created. All relevant factors and their evaluation methods are shown in Table 1 of Section 4. After 2004, some of the cavity chamber conversion and correction factors have been re-evaluated on three occasions.

## 1.2 MAY 2006 – FEBRUARY 2014

Refined MC simulations, as described in NPL report DQL-RD 004 (Sander and Nutbrown 2006), were performed at the beginning of 2006, leading to a revised set of MC calculated conversion and correction factors for the cavity chamber TH100C, as shown in column 4 of Table 1 in Section 4. The stem scatter, polarity and ion recombination correction factors, and the combined air attenuation and scatter correction factor were derived by refined measurements. The overall correction factor for NPL's HDR $^{192}$Ir primary standard changed by +0.16% in May 2006.

1.3 MARCH 2014 – JUNE 2019

The next revision of correction factors was carried out in 2014, when the type of HDR $^{192}$Ir radiation source used at NPL was changed from the Nucletron microSelectron-v1 classic source to the Elekta Flexisource. All previously calculated correction factors were adopted at this stage. However, the separately reported central electrode correction factor of 0.9984 was removed from the list (resulting in a change of +0.16%) because it was already included in the wall correction factor. The correction factors for stem scatter, polarity correction, and air attenuation and scatter were re-evaluated by measurement. The overall correction factor for NPL's HDR $^{192}$Ir primary standard changed by +0.26% in March 2014.

1.4 FROM JULY 2019

Pre-July 2019 calibrations for HDR $^{192}$Ir at NPL were based on data from ICRU report 37 (ICRU 1984). In July 2019, a further revision of conversion and correction factors was implemented (see Table 1, Section 4). The +0.27% change in the overall correction factor for NPL's HDR $^{192}$Ir primary standard due to the measured catheter attenuation correction was almost completely compensated by the –0.23% overall change in the three re-evaluated Monte Carlo calculated conversion and correction factors. The latter change was necessary because of the inclusion of the stem scatter correction factor in the wall correction factor and the implementation of the recommendations of ICRU report 90 (ICRU 2016). A small adjustment of +0.01% was also made to the density of dry air. The air density appears in the denominator of the measurement equation, resulting in a change of -0.01% in the primary standard chamber factor.
The overall correction factor for NPL's HDR $^{192}$Ir primary standard changed by +0.03% in July 2019.

## 2 CAVITY THEORY FOR THE $^{192}$IR AIR KERMA STANDARD

A cavity ionisation chamber consists of a chamber wall and a small gas-filled cavity of volume $V$. If the chamber is irradiated by a beam of uncharged particles (here: photons), secondary electrons are produced in the chamber wall and those electrons passing through the cavity will transfer some of their energy by ionising the gas inside the cavity, producing a charge, $Q$, which can be measured. The charge measured with a cavity chamber under ideal conditions, i.e. without the ionisation chamber being present, can be related to the air kerma at a reference point, $P$, free in air by applying cavity theory. Figure 1 shows a large volume of air being irradiated by a broad parallel polyenergetic photon beam.

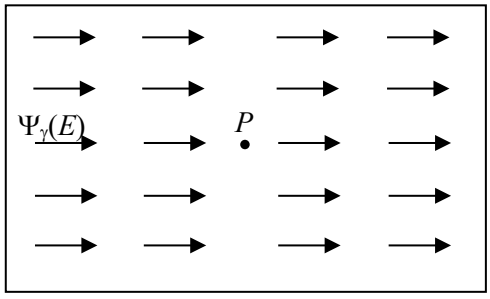


**Figure 1. A measurement point, $P$, is considered inside a large volume of air, which is irradiated by a broad parallel polyenergetic photon beam with photon energy fluence $\Psi_\gamma(E)$.**

The air kerma, in air, at point $P$ is given by

$$K_{\text{air}} = \int_0^{E_{\max}} \Psi_\gamma(E) \left(\frac{\mu_{\text{tr}}(E)}{\rho}\right)_{\text{air}} dE = \int_0^{E_{\max}} \Psi_\gamma(E) \left(\frac{\mu_{\text{en}}(E)}{\rho}\right)_{\text{air}} \frac{1}{1-\bar{g}_{\text{air}}} dE \ , \quad (1)$$

where $\Psi_\gamma(E)$ is the distribution of the photon energy fluence (units: J m$^{-2}$) differential in energy, $\left(\frac{\mu_{\text{tr}}(E)}{\rho}\right)_{\text{air}}$ is the mass-energy transfer coefficient of air (units: m$^2$ kg$^{-1}$), $\left(\frac{\mu_{\text{en}}(E)}{\rho}\right)_{\text{air}}$ is the mass-energy absorption coefficient of air and $\bar{g}_{\text{air}}$ is the fraction of energy of the secondary electrons liberated by photons lost to bremsstrahlung in air.
For the measurement of photons with energies greater than 350 keV, free-air chambers are not suitable because some correction factors and the associated uncertainties become unacceptably large (Büermann and Burns 2009).
If radiation beams contain higher energy photons, e.g. photons which can be found in the $^{192}$Ir spectrum, cavity chambers are used to realise air kerma. Figure 2 shows a cavity chamber with a graphite wall placed inside a large air volume with the geometric centre of the air cavity at the reference point, $P$.

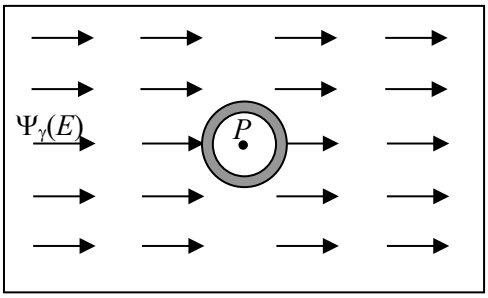


**Figure 2. A graphite-walled cavity ionisation chamber is placed inside a large volume of air, with the cavity volume centred on the reference point, $P$. It is assumed that the photon energy fluence, $\Psi_\gamma(E)$, is the same as in Figure 1.**

The wall of the cavity chamber must be thick enough to prevent secondary electrons liberated by photon interactions outside the wall material from entering the cavity and the wall is assumed to be thin enough so that the photon energy fluence is not disturbed. Once charged particle equilibrium (CPE) has been established in the graphite wall, the dose to the graphite wall, $D_{\text{graphite}}$, can be written as

$$D_{\text{graphite}} \overset{\text{CPE}}{=} K_{\text{graphite}} \cdot \left(1 - \bar{g}_{\text{graphite}}\right) = \int_0^{E_{\max}} \Psi_\gamma(E) \left(\frac{\mu_{\text{en}}(E)}{\rho}\right)_{\text{graphite}} dE \ , \quad (2)$$

where $K_{\text{graphite}}$ is the graphite kerma, $\bar{g}_{\text{graphite}}$ is the fraction of energy lost to bremsstrahlung, $\left(\frac{\mu_{\text{en}}(E)}{\rho}\right)_{\text{graphite}}$ is the mass-energy absorption coefficient of graphite and $\Psi_\gamma(E)$ is the photon energy fluence which is assumed to be the same as in Equation 1 (see also Figures 1 and 2).
There will be CPE inside the air cavity if the size of the cavity is small compared to the maximum range of the secondary electrons. The absorbed dose in the air cavity, $D_{\text{air}}$, is then given by

$$D_{\text{air}} \overset{\text{CPE}}{=} K_{\text{air}} \cdot (1 - \bar{g}_{\text{air}}) = \frac{Q}{m_{\text{air}}} \cdot \frac{\bar{W}_{\text{air}}}{e} \ , \quad (3)$$

where $Q$ is the charge produced by ionisation in the air cavity, $m_{\text{air}}$ is the mass of air in the cavity and $(\bar{W}_{\text{air}}/e) = (33.97 \pm 0.12)$ J C$^{-1}$ is the average energy in joules required to produce

an ion pair in dry air per unit charge released (ICRU 2016).
The Bragg-Gray conditions state that:
(a) the cavity must be small in comparison with the range of the secondary electrons set in motion by photon interactions in the chamber wall, so that the cavity does not perturb the electron fluence, i.e. $\Phi_{e^-}^{\text{graph.}}(E) = \Phi_{e^-}^{\text{air}}(E) = \Phi_{e^-}(E)$, and (b) the absorbed dose in the cavity is assumed to be deposited entirely by the charged particles crossing it, i.e. photon interactions inside the cavity are assumed to be negligible.
Bragg-Gray cavity theory relates the ionisation per unit mass in a small air cavity to the energy absorbed per unit mass in the surrounding medium (here: graphite). The ratio of the absorbed dose to the graphite wall, $D_{\text{graphite}}$, and the absorbed dose to the air cavity, $D_{\text{air}}$, is

$$\frac{D_{\text{graphite}}}{D_{\text{air}}} = \frac{\int_0^{E\text{max}} \Phi_{e^-}(E)\,(S(E)/\rho)_{\text{graphite}}\,\text{d}E}{\int_0^{E\text{max}} \Phi_{e^-}(E)\,(S(E)/\rho)_{\text{air}}\,\text{d}E} = \left(\frac{\bar{S}}{\rho}\right)_{\text{air}}^{\text{graphite}}, \tag{4}$$

where $(S(E)/\rho)$ is the distribution of the mass stopping power differential in energy and $(\bar{S}/\rho)_{\text{air}}^{\text{graphite}}$ is the ratio of the mean electron-fluence weighted mass collision stopping powers of graphite and air.
Equation 1 divided by Equation 2 gives

$$\frac{K_{\text{air}}}{D_{\text{graphite}}} = \frac{\int_0^{E\text{max}} \Psi_\gamma(E)\,(\mu_{\text{en}}(E)/\rho)_{\text{air}}\,(1/(1-\bar{g}_{\text{air}}))\,\text{d}E}{\int_0^{E\text{max}} \Psi_\gamma(E)\,(\mu_{\text{en}}(E)/\rho)_{\text{graphite}}\,\text{d}E} = \left(\frac{\bar{\mu}_{\text{en}}}{\rho}\right)_{\text{graphite}}^{\text{air}} \cdot \frac{1}{1-\bar{g}_{\text{air}}}, \tag{5}$$

where $(\bar{\mu}_{\text{en}}/\rho)_{\text{graphite}}^{\text{air}}$ is the ratio of the mean photon-fluence weighted mass-energy absorption coefficients of air and graphite.

Combining Equations 4 and 5 leads to

$$K_{\text{air}} = D_{\text{air}} \cdot \left(\frac{\bar{\mu}_{\text{en}}}{\rho}\right)_{\text{graphite}}^{\text{air}} \cdot \frac{1}{1-\bar{g}_{\text{air}}} \cdot \left(\frac{\bar{S}}{\rho}\right)_{\text{air}}^{\text{graphite}}, \tag{6}$$

and combining this with Equation 3 yields

$$K_{\text{air}} = \frac{Q}{m_{\text{air}}} \cdot \frac{\bar{W}_{\text{air}}}{e} \cdot \left(\frac{\bar{\mu}_{\text{en}}}{\rho}\right)_{\text{graphite}}^{\text{air}} \cdot \frac{1}{1-\bar{g}_{\text{air}}} \cdot \left(\frac{\bar{S}}{\rho}\right)_{\text{air}}^{\text{graphite}}. \tag{7}$$

Equation 7 relates the charge measured with a cavity chamber under ideal conditions to the air kerma at the reference point, $P$.
For non-ideal (realistic) conditions, correction factors, which will be discussed in Section 3, must be applied to Equation 7.

## 3 CAVITY CHAMBER CORRECTION FACTORS

In Section 3.1, the Monte Carlo calculated correction factor, $F_{\text{MC}}$, will be defined. Section 3.2 describes the measurement equation for the $^{192}$Ir reference air kerma rate primary standard. The determination of the correction factors and the associated uncertainties will be discussed in detail in Sections 3.3.5 and 3.4, and then summarised in Sections 4 and 5.
NPL's HDR $^{192}$Ir RAKR primary standard comprises both a graphite-walled cavity ionisation chamber based on Bragg-Gray and large cavity theory, and a lead collimator for the $^{192}$Ir source. Monte Carlo methods were used to derive perturbation correction factors to account for deviations from ideal Bragg-Gray conditions.
For a detailed description of the RAKR measurement setup, see Section 3 of NPL report DQL-RD 004 (Sander and Nutbrown 2006). For the following discussion and for

convenience, two of the figures from the previous report showing a side view and a top view of the measurement setup are also shown in Figures 3 and 4.

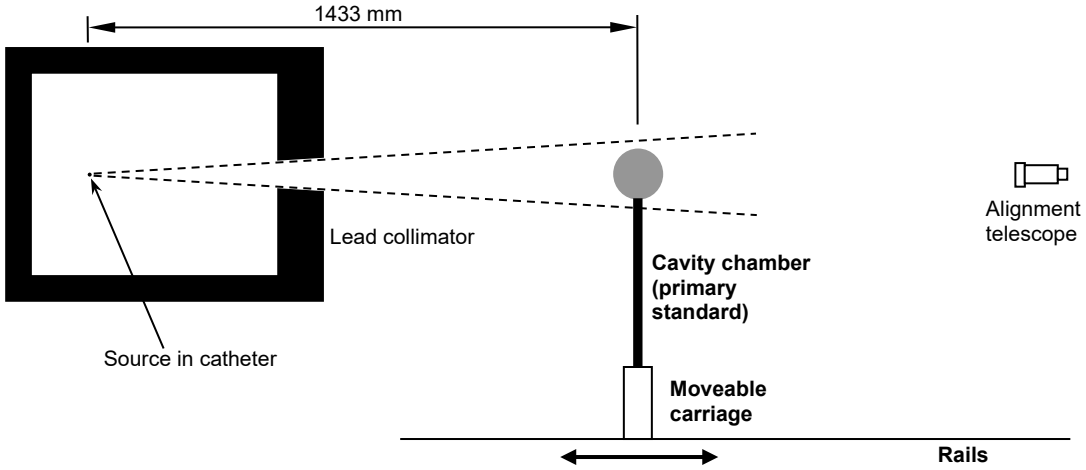


**Figure 3. Setup for HDR $^{192}$Ir source calibrations at NPL, side view (not to scale)**

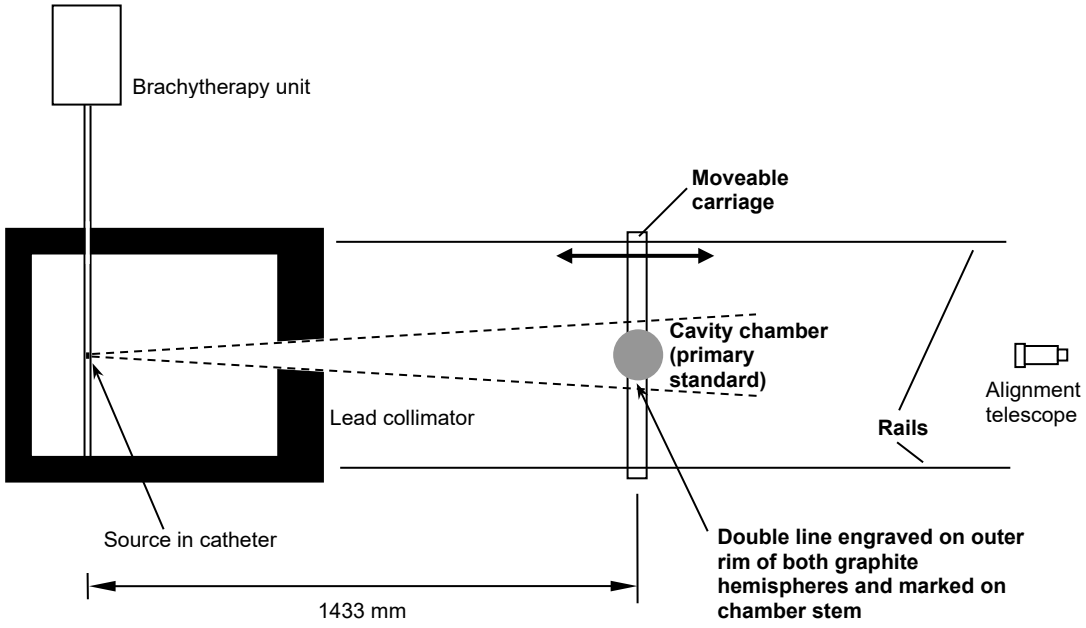


**Figure 4. Setup for HDR $^{192}$Ir source calibrations at NPL, top view (not to scale)**

## 3.1 DEFINITION OF THE MONTE CARLO CALCULATED CORRECTION FACTOR $F_{MC}$

Air kerma, $K_{air}$, is determined from a measurement of the ionisation charge in the cavity chamber and $K_{air}$ is defined as

$$K_{air} = \frac{Q_{meas}}{m_{air}} \cdot \frac{\bar{W}_{air}}{e} \cdot F \ , \tag{8}$$

where $Q_{meas}$ is the charge collected, $m_{air}$ is the known mass of air in the cavity, $(\bar{W}_{air}/e)$ is the average energy required to produce an ion pair in dry air per unit charge released and $F$ is the overall chamber correction factor. $F$ can be expressed as a product of factors, where each individual factor is equivalent to a certain physical effect. For the realisation of air

kerma, the total charge produced by ionisation in the air cavity, $Q$, needs to be determined. However, this cannot be measured directly. The charge, $Q$, is given by

$$Q = Q_{\text{meas}} \cdot k_{\text{ion}} \cdot k_{\text{pol}} \cdot k_{\text{stem}} \cdot k_{\text{mat}} \cdot k_{\text{conf}} \,, \tag{9}$$

where $k_{\text{ion}}$ is the correction factor for lack of saturation due to ion recombination, $k_{\text{pol}}$ is the polarity correction factor, $k_{\text{stem}}$ is the stem scatter correction factor, $k_{\text{mat}}$ is the non-graphite materials correction factor (for non-graphite materials near the tip of the chamber stem) and $k_{\text{conf}}$ is the configuration correction factor, also known as dead volume correction factor. $k_{\text{ion}}$ and $k_{\text{pol}}$ were determined by measurement. For this evaluation, $k_{\text{stem}}$ and $k_{\text{mat}}$ were not calculated as separate factors but included in the Monte Carlo calculated wall correction factor $k_{\text{wall}}$ (see Equations 14 and 19).

For all pre-July 2019 evaluations of chamber correction factors for chamber TH100C, $k_{\text{mat}}$ was estimated to be unity. Borg *et al.* (2000) showed that non-graphite materials used for the construction of cavity chambers, e.g. insulators and holders, can have a substantial effect on the ion chamber response and should be included in the correction factors for a primary standard of air kerma. The material effect for NPL's 1.7 cm$^3$ cylindrical graphite-walled cavity chambers SCB1, SCA2 and SCA3, used for the measurement of $^{60}$Co and $^{137}$Cs, was determined by Monte Carlo simulations by Duane *et al.* (2009) and found to be 0.3%. The surface of the insulator between the central electrode and the cylindrical graphite cap was 11% of the inside surface of the cylindrical graphite cap facing the air cavity. Based on these figures, the material effect correction factor, $k_{\text{mat}}$, for the spherical cavity chamber TH100C was estimated to be negligible because the surface area of the amber insulator between the central electrode and the spherical graphite wall is only 1% of the total inside surface of the graphite sphere facing the air cavity. The chemical composition of the graphite equivalent insulators used in the chamber stems of both the spherical cavity chamber and the cylindrical chambers are similar. No uncertainty was assigned to the material effect correction factor for chamber TH100C.

For the spherical geometry of cavity chamber TH100C, due to the absence of sharp corners on the conducting surfaces, the effective collecting volume was assumed to be identical to the geometric volume of the air cavity. The likely dead volume in the vicinity of the surface of the amber insulator which faces the collecting volume between the collecting electrode and the spherical graphite wall was found to be negligible by analysing the shape of the electric field lines inside the collecting volume, resulting in a configuration correction factor[1], $k_{\text{conf}}$, of unity (Sander and Nutbrown 2006). No uncertainty was assigned to the configuration correction.

Equation 7 in Section 2, which follows from Bragg-Gray cavity theory, relates the charge measured with a cavity chamber under ideal conditions to the air kerma at the reference point, $P$. For realistic conditions, correction factors, which correct for the deviation from ideal Bragg-Gray conditions by considering the actual measurement setup and the chamber geometry, must be applied to Equation 7. The HDR brachytherapy primary standard cavity chamber TH100C collects charged particles which are produced by photons scattering in the graphite wall. Compton electrons produced in the chamber wall enter the air cavity and ionise the air inside the cavity volume. However, the chamber wall attenuates the incident photons, scattered photons can produce secondary electrons which produce further ionisation in the

[1] The configuration correction factor, $k_{\text{conf}}$, needs to be considered in cavity chambers, where two conducting surfaces meet at different angles. For cylindrical cavity chambers, the effective collecting volume is smaller than the geometric volume of the cavity because the electric field strength near the corners of the graphite cap is $|\vec{E}| \cong 0$. Charged particles generated in this region will therefore not contribute to the collected ionisation current and a configuration correction factor greater than unity will have to be applied to the measured current. For the old NPL air kerma primary standard for $^{137}$Cs and $^{60}$Co, which comprised a set of three cylindrical cavity chambers with nominal cavity volumes of 1.7 cm$^3$ each, the configuration correction (also known as dead volume correction) was determined experimentally and found to be 0.1% (Barnard *et al.* 1959, Barnard *et al.* 1964).

chamber cavity, and the chamber material near the cavity has a density which is different to that of air. It is also possible for a photon to scatter twice and the knock-on electron from the second scatter event to contribute to ionisation.
Combining Equations 8 and 9 and introducing a correction factor, $F_{\mathrm{MC}}$, which was determined by Monte Carlo simulations, gives

$$K_{\mathrm{air}} = \frac{Q}{m_{\mathrm{air}}} \cdot \frac{\bar{W}_{\mathrm{air}}}{e} \cdot F_{\mathrm{MC}} = D_{\mathrm{air}} \cdot F_{\mathrm{MC}} \ , \tag{10}$$

where $D_{\mathrm{air}}$ is the absorbed dose to the air cavity of the cavity chamber (see Equations 3, 6 and 7).
The correction factor, $F_{\mathrm{MC}}$, can be expressed as a ratio

$$F_{\mathrm{MC}} = \frac{K_{\mathrm{air}}}{D_{\mathrm{air}}} \ , \tag{11}$$

where the quantity in the numerator is the air kerma, free in air, for a given photon beam at the measurement point $P$ (see Figure 1), which coincides with the position of the geometric centre of the air cavity of the cavity chamber. This was directly calculated by Monte Carlo simulation. $D_{\mathrm{air}}$ in the denominator is equivalent to the Monte Carlo calculated term $D_{\mathrm{cav,\,real}}(\mathrm{total})$, which is the total dose to the air cavity of the actual cavity chamber as described in Section 3.3.5. This is based on the assumption that $m_{\mathrm{air}}$ and $\bar{W}_{\mathrm{air}}/e$ in Equation 10 are constants and $D_{\mathrm{air}}$ is proportional to $Q$. The MC model of the cavity chamber included the graphite sphere, central graphite electrode and air inside the cavity. The 1.35 cm long graphite boss of the threaded hemisphere plus an additional 1 cm length of the chamber stem, including all non-graphite materials, were also included in the MC model. The correction factor, $F_{\mathrm{MC}}$, can be factorised and interpreted in a way that matches cavity theory analysis (see Equations 13 and 14).

## 3.2 MEASUREMENT EQUATION FOR THE $^{192}$IR REFERENCE AIR KERMA RATE PRIMARY STANDARD

Reference air kerma rate has been defined by the International Commission on Radiation Units and Measurements (ICRU) as the kerma rate to air, in air, at a reference distance of 1 m, corrected for air attenuation and scattering (ICRU 1985, ICRU 1997). For elongated brachytherapy sources, such as the HDR $^{192}$Ir Flexisource, the reference point lies on the perpendicular bisecting plane, i.e. the plane normal to and bisecting the long axis of the source (ICRU 2004).
The following measurement equation for NPL's HDR $^{192}$Ir primary standard shows how the reference air kerma rate of an HDR $^{192}$Ir source is determined from the measured ionisation current in the cavity chamber, when using the measurement setup shown in Figures 3 and 4. The following equation combines Equations 9 and 10 and considers the definition of reference air kerma rate:

$$\dot{K}_R = \frac{(Q_{\mathrm{raw}} - Q_{\mathrm{leakage}}) \cdot k_{\mathrm{elec}}}{t \cdot \rho_{\mathrm{air}} \cdot V_{\mathrm{air}}} \cdot \frac{\bar{W}_{\mathrm{air}}}{e} \cdot k_{\mathrm{ion}} \cdot k_{\mathrm{pol}} \cdot k_{\mathrm{conf}} \cdot k_{\mathrm{aasc}} \cdot k_{\mathrm{catheter}} \cdot \left(\frac{d}{d_{\mathrm{ref}}}\right)^2 \cdot k_{\mathrm{dec}} \cdot k_{Tp} \cdot k_h \cdot F_{\mathrm{MC}} \ , \tag{12}$$

where
$\dot{K}_R$ is the reference air kerma rate expressed in Gy s$^{-1}$ at 1 m,
$Q_{\mathrm{raw}}$ is the charge displayed on the electrometer after exposing the cavity chamber to the HDR $^{192}$Ir Flexisource for time $t$,
$Q_{\mathrm{leakage}}$ is the leakage charge measured with the electrometer after time $t$,
$k_{\mathrm{elec}}$ is the electrometer calibration coefficient in terms of coulombs (C) per displayed coulombs ('C'),
$t$ is the exposure time (s),

$\rho_{air}$ = 1.2046 kg m$^{-3}$ is the density of dry air at a standard temperature of 20 ºC and a standard pressure of 1013.25 mbar (Picard *et al.* 2008),
$V_{air}$ = 1.02519E-04 m$^3$ is the measured air cavity volume and
$\overline{W}_{air}/e$ is the average energy required to produce an ion pair in dry air per unit charge released, where $\overline{W}_{air}/e$ = (33.97 ± 0.12) J C$^{-1}$ (ICRU 2016). The uncertainty is given in the form of one standard deviation.
$k_{ion}$ is the ion recombination correction factor (determined by measurement),
$k_{pol}$ is the polarity correction factor (determined by measurement),
$k_{conf}$ = 1.0000 is the configuration correction factor (see Section 3.1),
$k_{aasc}$ is the combined air attenuation and scatter correction factor which corrects the measured ionisation current at the centre-to-centre source-to-chamber distance $d$ = 1.433 m for air attenuation and scatter due to the air column between the source and the point of measurement,
$k_{catheter}$ is the catheter attenuation correction factor which corrects the measured ionisation current for the attenuation of the photons from the encapsulated HDR $^{192}$Ir source by the polyamide (= nylon) catheter (type 5F LumenCare Azure, measured inner diameter = 1.23 mm, measured outer diameter = 1.68 mm) inside the lead castle,
$\left(\frac{d}{d_{ref}}\right)^2$ is the inverse square correction factor to normalise the ionisation current measured at $d$ = 1.433 m to the reference distance $d_{ref}$ = 1 m,
$k_{dec}$ is the decay correction factor which corrects the measured ionisation current at time $t$ to the reference time $t_{ref}$,
$k_{Tp} = (273.15 + T)/(273.15 + T_0) \cdot p_0/p$ is the air density correction factor correcting the measured ionisation current to standard atmospheric conditions, where $T_0$ = 20 °C,
$T$ = measured air temperature in °C, $p_0$ = 1013.25 mbar and $p$ = measured air pressure in mbar,
$k_h$ = 0.9970 is the humidity correction factor which accounts for the effect of humidity (ambient water vapour, 20% to 70% relative humidity) on $\overline{W}_{air}$ (Rogers and Ross 1988) and
$F_{MC}$ is the Monte Carlo calculated correction factor.

When secondary standard ionisation chambers are calibrated against the primary standard by using the calibrated HDR $^{192}$Ir source, the ionisation current of the secondary standard must be corrected for source decay to the same reference time, $t_{ref}$, to calculate the calibration coefficient, i.e. the RAKR measured with the primary standard divided by the secondary standard response.

## 3.3 MONTE CARLO CALCULATED CORRECTION FACTORS

Some of the primary standard correction factors were evaluated by calculation using Monte Carlo techniques. This section gives an overview of the Monte Carlo codes used and describes the methods used for determining the correction factors.

### 3.3.1 Monte Carlo codes

The Monte Carlo simulations described in this report were performed using the usercodes BEAMnrc and *cavity* that form part of the EGSnrc code system; release 2018 from GitHub (Kawrakow *et al.* 2018a). BEAMnrc is a general-purpose code for modelling sources of radiation such as linear accelerators and radioactive sources (Rogers *et al.* 2018) and was used here to model NPL's Elekta HDR $^{192}$Ir Flexisource and associated lead collimator. The C++ application *cavity* is an advanced code for calculating the dose response of an ionisation chamber (Kawrakow *et al.* 2018b) and offers several features and variance reduction techniques for determining chamber correction factors. All simulations using these codes were performed on a local Linux computing cluster.

### 3.3.2 Material datasets

The datasets for all required materials in this work were generated using the pre-processing code PEGS4 (Kawrakow *et al.* 2018a). The IAPRIM (Rogers *et al.* 1989) and EPSTFL (Duane *et al.* 1989) options were enabled to ensure that both collisional and radiative stopping powers matched those given in ICRU report 37 (ICRU 1984). The density effect corrections required for input to PEGS4 were obtained using the program ESTAR (Berger *et al.* 2005), version 2.0.1 (July 2017). To implement the recommendations of ICRU report 90 (ICRU 2016), the datasets for all graphite materials were generated using a mean excitation energy ($I$ value) of 81.0 eV and the density effect corrections for this material were derived using the crystalline density of graphite (2.265 g $cm^{-3}$) instead of the bulk density. For all other materials, the default $I$ value was used together with density effect corrections based on the bulk density of that material. The material datasets required for the air-equivalent and graphite-equivalent chamber geometries were obtained in a similar way with only the bulk density of the air and graphite material being changed in each case (the same density effect corrections as used for normal air and graphite were used throughout). The electron and photon threshold energies used in PEGS4 were set to 0.521 MeV and 0.01 MeV, respectively, in all cases.

### 3.3.3 Calculation of the shielded $^{192}$Ir spectrum from an Elekta HDR $^{192}$Ir Flexisource

BEAMnrc was used to determine the gamma spectrum from an Elekta HDR $^{192}$Ir Flexisource (model designation: 136.147) inside a 5F LumenCare Azure nylon catheter (part number: 110689-01; measured inner diameter: 1.23 mm, measured outer diameter: 1.68 mm) after collimation by the lead castle. Due to limitations in the geometry definition of the component module SIDETUBE within BEAMnrc, the source was approximated to a concentric cylindrical geometry that included the iridium active source material, the stainless steel encapsulation and polyamide catheter (with corresponding air gaps) but excluded the shielding at either ends of the source. The previous work with a Nucletron microSelectron-v1 classic HDR $^{192}$Ir source used a similar approximation and found that this made no significant difference to the spectral output and estimated the consequential effect on the overall chamber correction factor to be no more than 0.1%. Both the front face (including aperture) and back wall of the lead collimator were also included in the model. The scoring plane where the full phase space of all particles is scored by BEAMnrc was positioned just upstream of the primary standard cavity chamber.

The $^{192}$Ir source spectrum (DDEP 2004) used for the simulations included photons directly following the β-decay and additionally K- and L-shell X-rays, contributing at least 0.1% to the $^{192}$Ir spectrum. The DDEP data usually represent the best available decay data for selected radionuclides (DDEP 2004, Pearce 2008). The default EGSnrc transport parameters were used with low energy physical processes also enabled, i.e. atomic relaxations, Rayleigh scattering, photoelectron angular sampling, bound Compton scattering and electron impact ionisation. The global electron and photon transport cut off energies ECUT and PCUT were set to 0.521 MeV and 0.01 MeV, respectively, in all regions in the source geometry.

### 3.3.4 Calculation of chamber response

The egs++ application *cavity* was used to simulate the response of the primary standard cavity chamber TH100C in the collimated radiation beam from the $^{192}$Ir brachytherapy source. An accurate geometric model of the cavity chamber and associated materials based on both metrological measurements and manufacturers' specifications, including 3.1 cm of the stem (measured from the surface of the amber insulator facing the collecting volume), was first constructed using the associated egs++ geometry package. This chamber geometry was then placed inside a large box of air with the centre of the chamber positioned at 143.3 cm from the source and the BEAMnrc scoring plane positioned just upstream of the chamber. A series of simulations were then performed to determine the total dose to the chamber cavity

regions with various geometry configurations (see Section 3.3.5) using the source model described in the previous section as a full BEAMnrc simulation source (EGS_BeamSource). The dose calculation type was set to *Awall* to determine total dose to the cavity under normal conditions, i.e. including photon attenuation and scatter, and to *Fano* to determine the total dose to the cavity without attenuation of incident photons and with scattered photons discarded.

For all chamber simulations, the default EGSnrc transport parameters were used with the low energy physical processes enabled (as in the previous section). In particular, the PRESTA-II electron step algorithm and EXACT boundary crossing algorithm (with default skin depth) were chosen with XCOM photon cross-sections from the National Institute of Standards and Technology (NIST). The impact of using renormalised photoelectric cross-sections discussed by ICRU report 90 (as opposed to unrenormalised data) on the dose ratios being determined in this work was considered not to be significant, i.e. within the type A dose uncertainties for $^{192}$Ir energies, and so were not used. The electron and photon transport cut off energies ECUT and PCUT were set to 0.521 MeV and 0.01 MeV, respectively. To improve the efficiency of the simulations, the photon splitting variance reduction technique was also employed with a splitting factor of 10. Simulations were typically run until a standard uncertainty (type A) of better than 0.1% was achieved on the calculated dose to the cavity.

Additional *cavity* simulations were also performed using the same parameters to check the self-consistency of MC transport algorithms in EGSnrc. Here, the total dose to the cavity (excluding photon attenuation and scatter) of the graphite-equivalent chamber in a vacuum box was determined in a plane parallel beam of monoenergetic 300 keV photons. The use of a chamber with a fully built-up wall thickness and graphite-equivalent materials enables the Fano theorem to be used and, with no photon attenuation and scatter, the dose per incident fluence in the cavity (in Gy cm$^2$) should be equal to the product of the mean spectrum energy and the mass-energy absorption coefficient of the graphite wall material, i.e. the collision kerma (Kawrakow 2000a, Kawrakow 2000b). An estimate of the latter value for the same graphite wall material and incident photon spectrum was obtained in a separate simulation using the usercode *g*, and agreement with the calculated dose per incident fluence in the cavity was obtained to within 0.1%.

### 3.3.5 Monte Carlo calculated correction factors for cavity chamber TH100C

The Monte Carlo calculated factor, $F_{\mathrm{MC}}$, (see Equations 11 and 12) was divided into the following components

$$F_{\mathrm{MC}} = \tilde{F} \cdot k_{\mathrm{an}} \cdot k_{\mathrm{rn}} \cdot (1 - \bar{g}_{\mathrm{air}})^{-1} \,, \tag{13}$$

where $k_{\mathrm{an}}$ is the axial non-uniformity correction factor (axial = in the direction of the beam axis) and $k_{\mathrm{rn}}$ is the radial non-uniformity correction factor (radial = perpendicular to the beam axis). Both factors are needed to correct the dose averaged over the entire cavity volume, which has been considered for the calculation of $\tilde{F}$, to the dose at a point at the geometric centre of the cavity. $\bar{g}_{\mathrm{air}}$ is the fraction of energy of the secondary electrons liberated by photons lost to bremsstrahlung in air. $k_{\mathrm{an}}$, $k_{\mathrm{rn}}$ and $\bar{g}_{\mathrm{air}}$ were all previously calculated for the microSelectron-v1 HDR $^{192}$Ir source using two different MC codes, DOSPHEREnrc and CAVRZnrc. These three correction factors were retained from previous work (Sander and Nutbrown 2006) because the numerical values of the three factors are not affected by the new ICRU 90 data, and any effect due to differences in the source geometries of the old microSelectron-v1 HDR $^{192}$Ir source and the new Elekta HDR $^{192}$Ir Flexisource would be negligible.
Only factor $\tilde{F}$ of Equation 13 was recalculated (and factorised for a type B uncertainty analysis) as

$$\tilde{F} = \left(\frac{\bar{\mu}_{\text{en}}}{\rho}\right)^{\text{air}}_{\text{graphite}} \cdot \left(\frac{\bar{S}}{\rho}\right)^{\text{graphite}}_{\text{air}} \cdot k_{\text{fl}} \cdot k_{\text{wall}} \,, \tag{14}$$

where $(\bar{\mu}_{\text{en}}/\rho)^{\text{air}}_{\text{graphite}}$ is the ratio of the mean mass-energy absorption coefficients of air and graphite, $(\bar{S}/\rho)^{\text{graphite}}_{\text{air}}$ is the ratio of the mean mass stopping powers of graphite and air averaged in the unperturbed fluence crossing the graphite-equivalent chamber, $k_{\text{fl}}$ is the fluence perturbation correction factor, correcting for the perturbation of the electron fluence by the air cavity and $k_{\text{wall}}$ is the wall correction factor, correcting for photon attenuation and scattering in the graphite wall, central electrode and stem of the cavity chamber. $\tilde{F}$ is the ratio of the dose to the air cavity volume in the absence of the cavity chamber, and the dose to the cavity in the realistic chamber. Monte Carlo simulations were performed using *cavity* to determine this ratio:

$$\tilde{F} = \frac{D_{\text{cav,air}}(\text{no att., no scatt.})}{D_{\text{cav,real}}(\text{total})} \,, \tag{15}$$

where $D_{\text{cav,air}}(\text{no att., no scatt.})$ is the dose to the cavity of the air-equivalent chamber (see Figure 5), where incident photons that interact in the chamber wall are not attenuated and scattered photons are discarded; $D_{\text{cav,real}}(\text{total})$ is the total dose to the air cavity of the actual chamber, i.e. including the effects of photon attenuation and scattering, with real materials modelled and with the central electrode being present (see Figure 8). The type A relative standard uncertainty of $\tilde{F}$ was found to be $u(\tilde{F}) =$ 0.10%, $k$ = 1. This was obtained by combining the standard deviations of the Monte Carlo simulations for the calculations of $D_{\text{cav,air}}(\text{no att., no scatt.})$ and $D_{\text{cav,real}}(\text{total})$.

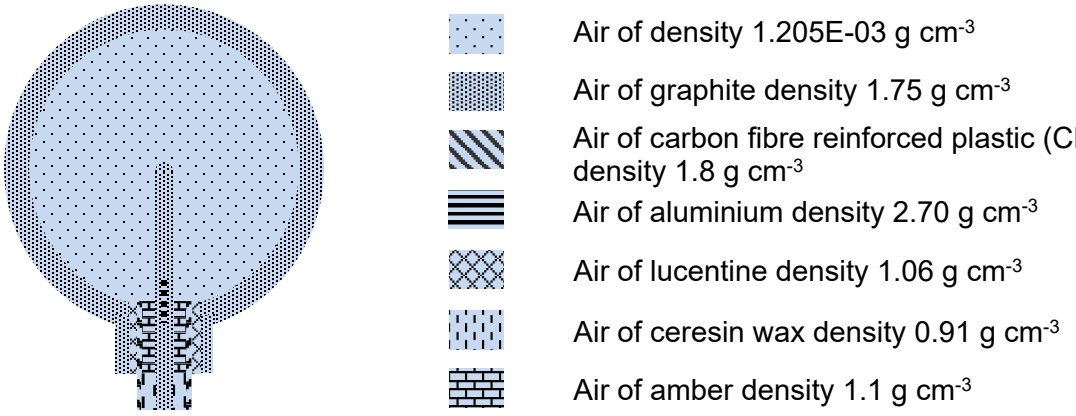


**Figure 5. Simulation geometry of the air-equivalent chamber, not to scale (no attenuation, no scatter)**

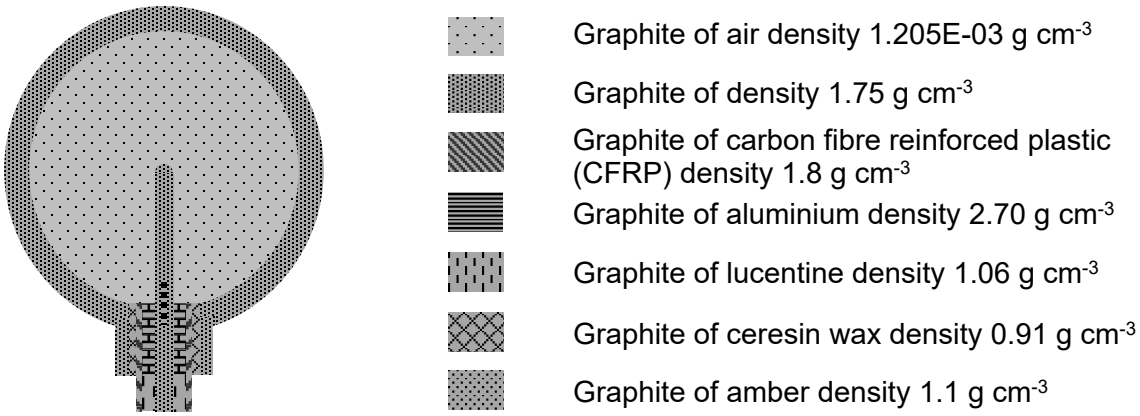


**Figure 6. Simulation geometry of the graphite-equivalent chamber, not to scale (no attenuation, no scatter)**

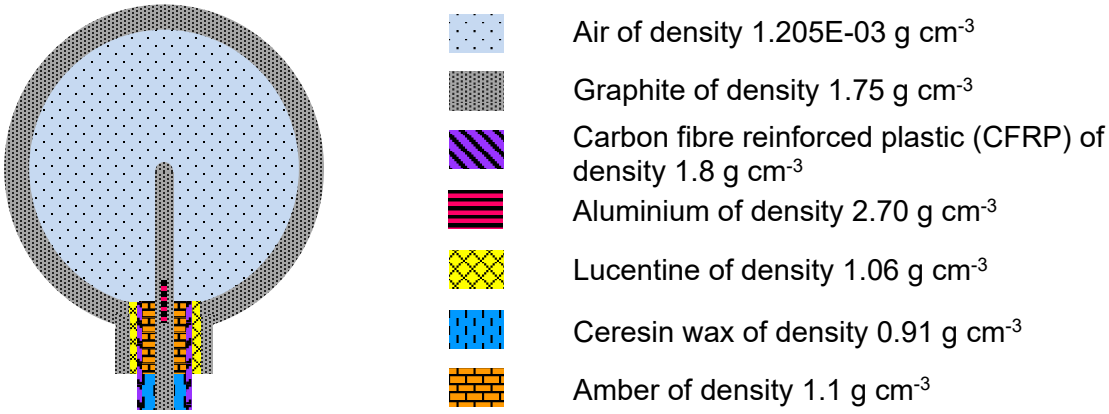


**Figure 7. Simulation geometry of the real chamber, not to scale (no attenuation, no scatter)**

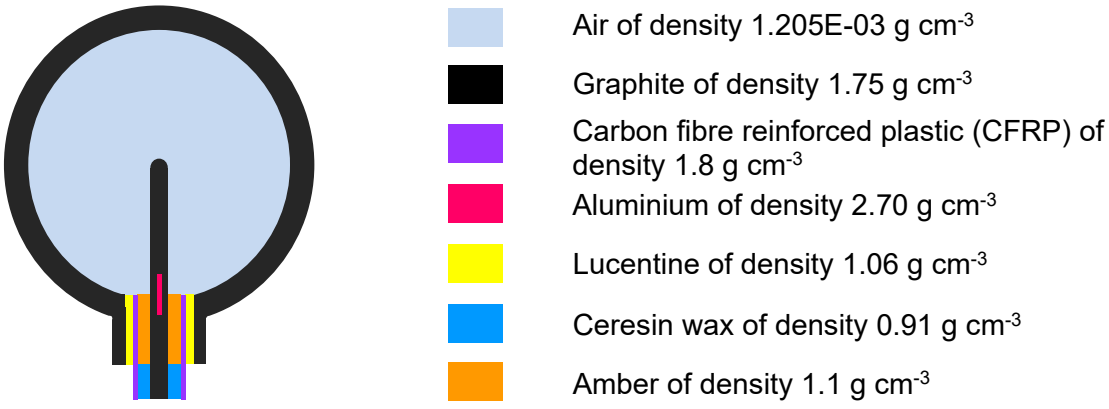


**Figure 8. Simulation geometry of the real chamber, not to scale (with attenuation, with scatter)**
**The top of the CFRP stem of the actual chamber was shortened by 1 mm and the gap was filled with Ceresin wax to isolate the chamber stem (guard electrode) from the collecting volume.**

For all four geometries shown in Figures 5 to 8, an inner radius of 2.90 cm and an outer radius of 3.29 cm were used for the spherical graphite shell.

Figure 9 is a schematic representation of the different components of correction factor $\tilde{F}$, as indicated in Equation 14 and using the chamber geometries shown in Figures 5 to 8. The individual factors were calculated by taking ratios of calculated cavity doses.

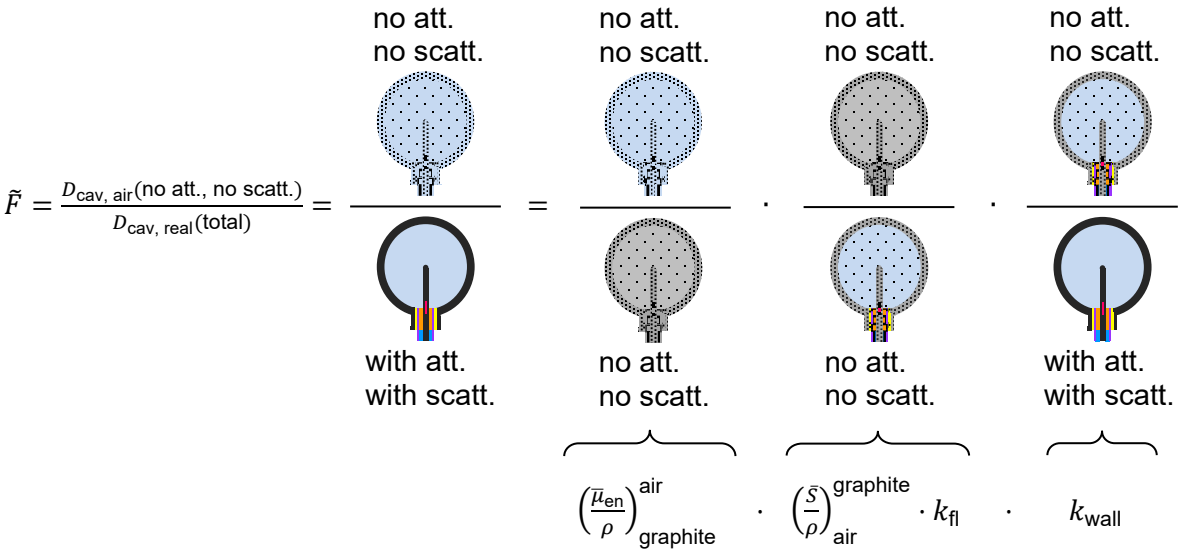


**Figure 9. Schematic representation of the factorisation of the correction factor $\tilde{F}$**

The ratio of the mass-energy absorption coefficients of air and graphite was calculated as follows (see also Section 2):

$$\left(\frac{\bar{\mu}_{\text{en}}}{\rho}\right)^{\text{air}}_{\text{graphite}} = \frac{D_{\text{cav, air}}\ (\text{no att., no scatt.})}{D_{\text{cav, graphite}}\ (\text{no att., no scatt.})} = \frac{\int_0^{E\text{max}} \Psi_\gamma(E)\ (\mu_{\text{en}}(E)/\rho)_{\text{air}}\ \text{d}E}{\int_0^{E\text{max}} \Psi_\gamma(E)\ (\mu_{\text{en}}(E)/\rho)_{\text{graphite}}\ \text{d}E}\ , \tag{16}$$

where $D_{\text{cav, graphite}}(\text{no att., no scatt.})$ is the dose to the cavity of a graphite-equivalent chamber where incident photons that interact in the chamber wall are not attenuated and scattered photons are discarded, and $\Psi_\gamma(E)$ is the photon energy fluence crossing the cavity. $(\bar{\mu}_{\text{en}}/\rho)^{\text{air}}_{\text{graphite}} = 1.0022$ with a type B relative standard uncertainty of $u\left((\bar{\mu}_{\text{en}}/\rho)^{\text{air}}_{\text{graphite}}\right) =$ 0.10%, $k$ = 1. The type B uncertainty analysis is consistent with the analysis for NPL's cavity chambers PS5-1 and PS5-2 reported by Duane *et al.* (2009).

The product of the ratio of the mass stopping powers of graphite and air and the fluence perturbation correction factor was calculated as a ratio of doses as follows:

$$\left(\frac{\bar{S}}{\rho}\right)^{\text{graphite}}_{\text{air}} \cdot k_{\text{fl}} = \frac{D_{\text{cav, graphite}}(\text{no att., no scatt.})}{D_{\text{cav, real}}(\text{no att., no scatt.})} = \frac{\int_0^{E\text{max}} \Phi_{e^-}^{\text{graph.}}(E)\ (S(E)/\rho)_{\text{graphite}}\ \text{d}E}{\int_0^{E\text{max}} \Phi_{e^-}^{\text{graph.}}(E)\ (S(E)/\rho)_{\text{air}}\ \text{d}E} \cdot k_{\text{fl}}\ , \tag{17}$$

where $D_{\text{cav,real}}(\text{no att., no scatt.})$ is the dose to the air cavity of the actual chamber with real materials modelled where the incident photons that interact in the chamber wall are not attenuated and scattered photons are discarded, and $\Phi_{e^-}^{\text{graph.}}(E)$ is the electron energy fluence crossing the cavity in the graphite-equivalent chamber.
The fluence perturbation correction factor, $k_{\text{fl}}$, corrects for the perturbation of the electron energy fluence by the air cavity in the real chamber (Bielajew 1986). The fluence perturbation correction factor in Equation 17 can be expressed as

$$k_{\text{fl}} = \frac{\int_0^{E\text{max}} \Phi_{e^-}^{\text{graph.}}(E)\ (S(E)/\rho)_{\text{air}}\ dE}{\int_0^{E\text{max}} \Phi_{e^-}^{\text{real}}(E)\ (S(E)/\rho)_{\text{air}}\ dE}\ , \tag{18}$$

where $\Phi_{e^-}^{\text{real}}(E)$ is the electron energy fluence crossing the cavity of the real chamber. $(\bar{S}/\rho)_{\text{air}}^{\text{graphite}} \cdot k_{\text{fl}} = 1.0061$ with a type B relative standard uncertainty of $u\left((\bar{S}/\rho)_{\text{air}}^{\text{graphite}} \cdot k_{\text{fl}}\right) =$ 0.08%, *k* = 1 (ICRU 2016).
The wall correction factor, correcting for photon attenuation and scattering in the graphite wall, central electrode and stem of the cavity chamber, was calculated as the ratio

$$k_{\text{wall}} = \frac{D_{\text{cav,real}}(\text{no att., no scatt.})}{D_{\text{cav,real}}(\text{total})}\,, \tag{19}$$

where $D_{\text{cav,real}}(\text{total})$ is the dose to the air cavity of the actual chamber with real materials modelled and with the incident photons being attenuated and scattered. $k_{\text{wall}} = 1.0417$ with a type B relative standard uncertainty of $u(k_{\text{wall}}) = 0.10\%$, *k* = 1. This type B uncertainty was estimated by examining the change in $k_{\text{wall}}$ by using two different methods: a direct $k_{\text{wall}}$ calculation and a calculation via dose ratios with the maximum observed spread in the two methods for determining $k_{\text{wall}}$ in the TH100C chamber simulation.
The final three factors in Equation 13, $k_{\text{an}}$, $k_{\text{rn}}$ and $(1-\bar{g}_{\text{air}})^{-1}$, and their type A and type B uncertainties, were retained from previous work (Sander and Nutbrown 2006). The axial non-uniformity correction factor, $k_{\text{an}}$, is required to account for the change in the spectrum over the chamber volume in the direction of the beam axis and a radial non-uniformity correction factor, $k_{\text{rn}}$, is required to account for the change in the spectrum over the chamber volume perpendicular to the beam axis (Bielajew 1990). The product of the two non-uniformity correction factors can be written as

$$k_{\text{an}} \cdot k_{\text{rn}} = \frac{K_{\text{coll}}}{D_{\text{cav,air}}(\text{no att., no scatt.})}\,, \tag{20}$$

where $K_{\text{coll}}$ is the collision kerma. $k_{\text{an}} = 0.9981$ with relative standard uncertainties of 0.05% (type A) and 0.10% (type B), *k* = 1. $k_{\text{rn}} = 1.0000$ with relative standard uncertainties of 0.01% (type A) and 0.02% (type B), *k* = 1.
The fraction of energy lost by bremsstrahlung can be expressed as the ratio of air kerma to collision kerma,

$$(1-\bar{g}_{\text{air}})^{-1} = \frac{K_{\text{air}}}{K_{\text{coll}}}\,, \tag{21}$$

which was determined by repeating Monte Carlo simulations of the air-equivalent chamber with bremsstrahlung switched off and taking ratios with and without bremsstrahlung production. This Monte Carlo calculated factor showed good agreement with tabulated values (Boutillon and Perroche 1985). $(1-\bar{g}_{\text{air}})^{-1} = 1.0007$ with relative standard uncertainties of 0.01% (type A) and 0.01% (type B), *k* = 1. Estimates for the type A and type B uncertainties in $(1-\bar{g}_{\text{air}})^{-1}$ were taken from Rogers ***et al.*** (1989).

The product of Equations 15, 20 and 21 results in an expression for $F_{\text{MC}}$ (see Equation 13), which is equivalent to Equation 11.

## 3.4 MEASURED CORRECTION FACTORS

### 3.4.1 Ion recombination correction factor

The correction factor for lack of saturation due to ion recombination, $k_{\text{ion}}$, is assumed to be energy independent for continuous and sparsely ionising radiation, such as the gamma radiation emitted by a typical HDR $^{192}$Ir brachytherapy source. The Niatel/Boutillon method (Boutillon 1998) was adopted to measure $k_{\text{ion}}$ as a function of ionisation current. Measurements were performed, for convenience, using an X-ray set. A general equation for $k_{\text{ion}}$ as a function of ionisation current was derived for cavity chamber TH100C and has been

retained from previous work (Sander and Nutbrown 2006). The ion recombination correction factor for cavity chamber TH100C which considers both initial recombination (constant) and volume recombination (dose rate dependent) can be calculated as

$$k_{\text{ion}} = 1.0025 + 1.57 \cdot 10^{7} \cdot I_V \ , \tag{22}$$

where $I_V$ is the measured ionisation current in A. The relative standard uncertainty in $k_{\text{ion}}$ was found through regression analysis, where $u(k_{\text{ion}}) = 0.02\%$, $k$ = 1.

### 3.4.2 Polarity correction factor

The standard operating voltage for cavity chamber TH100C is +500 V, applied to the central (collecting) electrode and the chamber stem (guard). The graphite sphere is earthed. The voltage gradient ensures that negative charge is being collected on the collecting electrode. The polarity correction factor was determined by changing the polarity of the polarising voltage and measuring the ionisation current with both positive and negative polarity high voltage on the central collecting electrode and guard electrode with respect to the earthed graphite sphere. This pair of measurements was repeated fifteen times. The negative ionisation currents collected with the collecting electrode at positive potential were found to be consistently higher than the positive ionisation currents.

The polarity correction factor was estimated using the following equation:

$$k_{\text{pol}} = \frac{I^{+}+I^{-}}{2 \cdot I^{+}} \ , \tag{23}$$

where $I^{+}$ is the ionisation current collected with the standard operating voltage (collecting electrode at +500 V) and $I^{-}$ is the ionisation current collected with the collecting electrode at -500 V.
The polarity correction factor, $k_{\text{pol}}$, was determined sixteen times, and the mean value was found to be $k_{\text{pol}} = 0.9995$ with a standard deviation of the mean of 0.02%. Only a type A uncertainty was assigned to $k_{\text{pol}}$, where $u(k_{\text{pol}}) = 0.02\%$, $k$ = 1.

### 3.4.3 Stem scatter correction factor

When chamber TH100C is irradiated at the calibration distance of 1433 mm, the collimated photon beam at the point of measurement (circular cross-section = 82 mm diameter) covers not only the whole graphite sphere (66 mm diameter) but also parts of the threaded graphite boss and the top of the chamber stem, leading to an increase in the number of scattered photons reaching the collecting volume and therefore an increase in the measured ionisation current. The stem scatter correction factor is defined as

$$k_{\text{stem}} = \frac{I_{\text{chamber only}}}{I_{\text{with dummy stem}}} \tag{24}$$

and corrects for the contribution of scattered photons from both the threaded boss of the graphite sphere and the top of the chamber stem. When chamber TH100C was initially commissioned as a primary standard, $k_{\text{stem}}$ could not be easily calculated using MC techniques because of limitations in the EGSnrc Monte Carlo code. Initially, $k_{\text{stem}}$ was therefore measured three times using a dummy stem (Sander and Nutbrown 2006). In 2014, when the primary standard cavity chamber was recommissioned for the Elekta HDR $^{192}$Ir Flexisource, $k_{\text{stem}}$ was measured sixteen times to improve the statistics on the data and the mean value was found to be $k_{\text{stem}} = 0.9974$ with a relative standard uncertainty of 0.07%, $k$ = 1.
For the evaluation of correction factors described in this NPL report, $k_{\text{stem}}$ was included in the MC calculated wall correction factor, $k_{\text{wall}}$. This was made possible because of improvements

made to the EGSnrc Monte Carlo code since the last evaluation of $k_{stem}$ in 2014. The application of a separate stem scatter correction factor is no longer required and $k_{stem}$ has been removed from the list of conversion and correction factors as of July 2019 (see Table 1, Section 4).

### 3.4.4 Air attenuation and scatter correction factor

For the realisation of RAKR, the kerma rate to air, in air, measured with cavity chamber TH100C, needs to be corrected for air attenuation and scatter between the brachytherapy source and the reference point at the centre of the cavity chamber (see definition of RAKR in Section 3.2.). The air attenuation and scatter correction factor [2], $k_{aasc}$, was measured by using a multiple distance method which was described in detail in NPL report DQL-RD 004 (Sander and Nutbrown 2006).

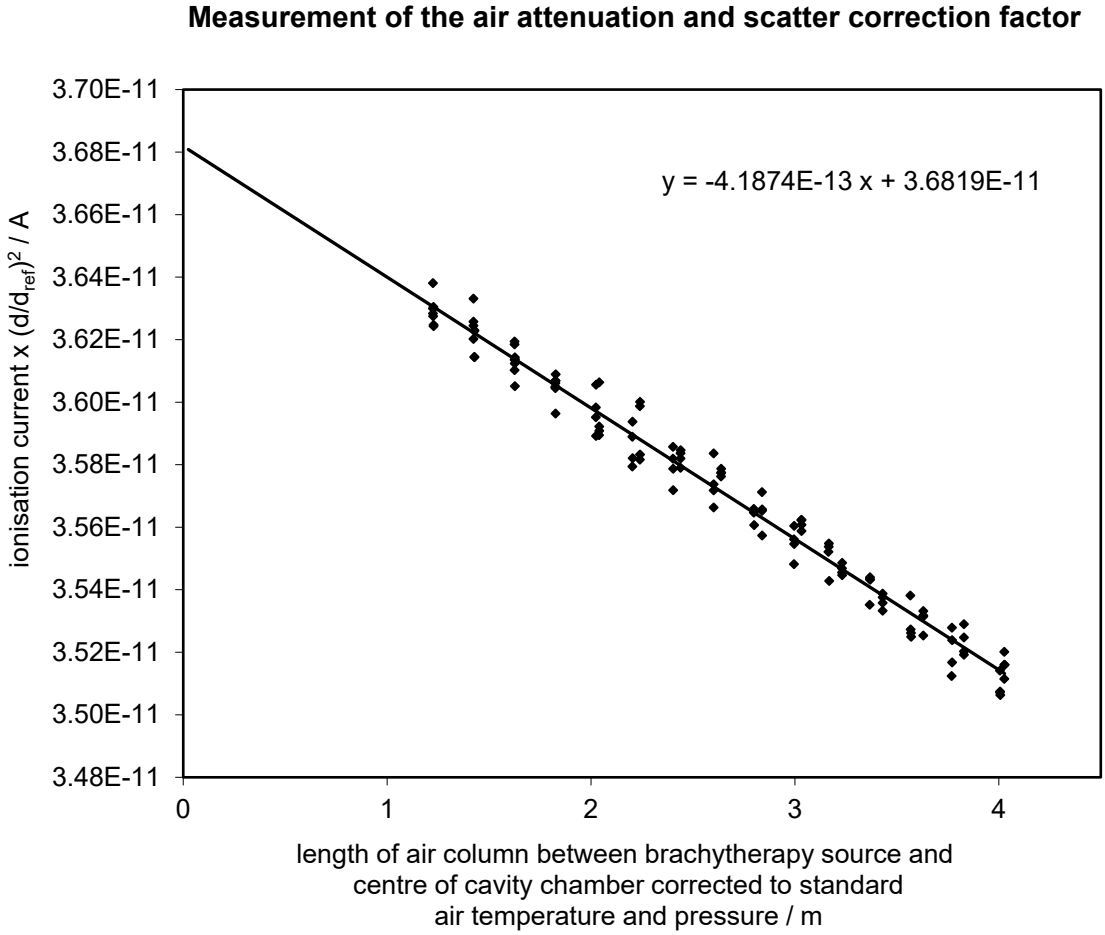


**Figure 10. Ionisation current as a function of the length of the air column between the HDR $^{192}$Ir source and the centre of the cavity chamber, corrected to standard air temperature and pressure and corrected for the inverse square dependence, where *d* is the distance shown on the x-axis and $d_{ref}$ = 1 m. A linear trendline has been fitted to all measurement points. The equation of this trendline is shown in the figure.**

The centre of the graphite sphere of the cavity chamber was aligned on the central beam axis of the collimated $^{192}$Ir photon beam. The centre of the cavity chamber was initially set up at 1.233 m distance from the centre of the $^{192}$Ir source and the ionisation current was

[2] In previous NPL publications, the symbol $k_{air}$ was used for the air attenuation and scatter correction factor.

measured and corrected for air temperature and pressure, ion recombination and source decay. Measurements of the ionisation current were then taken at 0.2 m increments with centre-to-centre source-to-chamber distances ranging from 1.233 m to 4.033 m. Figure 10 shows the results of the multiple distance measurements using an Elekta HDR $^{192}$Ir Flexisource during the recommissioning of the primary standard in 2013/2014.
All the different measured distances from the centre of the $^{192}$Ir source to the centre of the cavity chamber (minus the thickness of the graphite sphere) for measured air temperatures $T$ and pressures $p$ were normalised to normal air temperature, $T_0$ = 20 °C, and normal air pressure, $p_0$ = 1013.25 mbar. This ensured that the air columns with the normalised lengths shown on the x-axis of Figure 10 for a given cross-sectional area contain the same number of air molecules, i.e. scatter and attenuation centres, like the actual air column during the multiple distance measurements at air temperature $T$ and pressure $p$.
The physical thickness of the graphite sphere was not included in the total source-to-chamber distance because the attenuation and scatter from the graphite sphere has already been accounted for by the MC calculated wall correction factor, $k_{\text{wall}}$.
The air attenuation and scatter correction factor for the standard setup of cavity chamber TH100C is the ratio of the normalised ionisation currents at 0 m (source centre) and for a 1.429 m long air column (equivalent to the centre-to-centre source-chamber distance of 1.433 m minus the thickness of the graphite cap). If the measurements are performed under STP conditions ($T_0$ = 20 °C, $p_0$ = 1013.25 mbar), $k_{\text{aasc}} = I(0\ \text{m})/I(1.429\ \text{m}) = 1.0165$, where $I(0\ \text{m})$ and $I(1.429\ \text{m})$ are the ionisation currents normalised to 1 m distance, calculated using the equation shown in Figure 10 for x = 0 m and 1.429 m, respectively. For other atmospheric conditions, $k_{\text{aasc}}$ can be calculated using the general expression

$$k_{\text{aasc}} = 1 + \left(0.0165 \cdot \frac{293.15}{(273.15+T)} \cdot \frac{p}{1013.25}\right), \tag{25}$$

where $T$ is the air temperature in °C and $p$ is the pressure in mbar.
The standard uncertainty in $k_{\text{aasc}}$ was found through regression analysis of the line fitted to all data points in Figure 10. The intercept was found to be 3.6819E-11 with a relative standard uncertainty of 0.04% and a sensitivity coefficient of -0.02. The gradient was found to be -4.1874E-13 with a relative standard uncertainty of 1.33% and a sensitivity coefficient of 0.02. The combined relative standard uncertainty of $k_{\text{aasc}}$ was calculated as $u(k_{\text{aasc}}) = \sqrt{(-0.02 \times 0.04\%)^2 + (0.02 \times 1.33\%)^2} = 0.02\%$, using the values in the spreadsheet. The contribution of the uncertainties in $T$ and $p$ (see Equation 25) to the total uncertainty of $k_{\text{aasc}}$ was found to be negligible.

### 3.4.5 Catheter attenuation correction factor

For the RAKR measurement at NPL, the HDR $^{192}$Ir source is inserted into a plastic catheter to position the source reproducibly inside the lead collimator. The RAKR of the encapsulated source, i.e. the cylindrical $^{192}$Ir source encapsulated in a stainless steel cylinder, needs to be measured. RAKR is defined *in vacuo*, which means that for the NPL measurement setup the measured ionisation current must not only be corrected for air attenuation and scatter between the source and the centre of the cavity chamber (see Section 3.4.4) but also for attenuation and scatter caused by the polyamide (= nylon) catheter. The effect of catheter attenuation has previously been assumed to be negligible.
From 2004 to 2013, 6F nylon catheters were used for the RAKR measurements. The influence of a Nucletron 6F Lumencath catheter (part number: 089.075) on the RAKR measurement was estimated with Monte Carlo simulations. The outside diameter (OD = 1.9694 mm) and inside diameter (ID = 1.4787 mm) of the 6F catheter were measured with a coordinate measuring machine and the average radial thickness was calculated as $d_{\text{6F\_catheter}}$ = (OD – ID)/2 = 0.2453 mm with a combined relative standard uncertainty of 0.5%. The catheter attenuation correction was found to be less than 0.08% with a type A uncertainty of 0.05% ($k$ = 1). The correction and its uncertainty were of the same order of

magnitude. It was therefore decided to assume a catheter attenuation correction factor of unity and to account for any catheter attenuation effect by assigning a 0.05% relative standard uncertainty and including this component in the uncertainty of the air attenuation and scatter correction factor.

Since 2014, Nucletron LumenCare Azure 5F nylon catheters (part number: 110689-01) have been used for RAKR measurements at NPL. The following dimensions of the 5F catheter were measured with a coordinate measuring machine: OD = 1.6812 mm, ID = 1.2342 mm, average radial thickness $d_{5F\_catheter}$ = 0.2235 mm with a combined relative standard uncertainty of 0.4%.

Due to the similar radial thicknesses of both types of catheters, the 0.05% relative standard uncertainty for any catheter attenuation affect was still included in the uncertainty budget and the catheter attenuation correction factor for the 5F catheter was still assumed to be unity until 1 July 2019.

The catheter attenuation correction factor for the Nucletron LumenCare Azure 5F nylon catheter was finally measured by placing additional polyamide 'PA6' nylon sheets[3] in the beamline between the HDR $^{192}$Ir Flexisource and the cavity chamber TH100C in front of the aperture of the lead collimator. The 'PA6' nylon sheets with a nominal thickness of 0.075 mm each were combined to stacks with three, six and nine sheets. The total thicknesses of these three stacks of nylon sheets (SDOM < 0.14%) were measured with a calibrated digital external micrometer.

Starting with NPL's standard setup for RAKR measurements, the cavity chamber was set up in front of the lead collimator at the usual centre-to-centre source-to-chamber distance of 1433 mm. An HDR $^{192}$Ir Flexisource was inserted into a Nucletron LumenCare Azure 5F nylon catheter and moved to the centre of the lead collimator. The mean ionisation current was measured from three separate source transfers to the same dwell position for each of the following nylon filter thicknesses:

1) 5F catheter only = 0.2235 mm
2) 5F catheter (0.2235 mm) + 'PA6' nylon sheets 1 to 3 (0.2380 mm) = 0.4615 mm
3) 5F catheter (0.2235 mm) + 'PA6' nylon sheets 4 to 9 (0.4678 mm) = 0.6913 mm
4) 5F catheter (0.2235 mm) + 'PA6' nylon sheets 10 to 18 (0.7108 mm) = 0.9343 mm
5) 5F catheter only = 0.2235 mm

The corrected mean ionisation currents from steps 2), 3) and 4) were then normalised to the corrected mean ionisation current from steps 1) and 5) and plotted as a function of the total thickness of nylon between the source and the ionisation chamber (see Figure 11).

[3] Polyamide – Nylon 6 (PA6) sheets from Goodfellow Cambridge Limited, Huntingdon, PE29 6WR, UK; ref. no. AM301075/1, nominal thickness = 0.075 mm

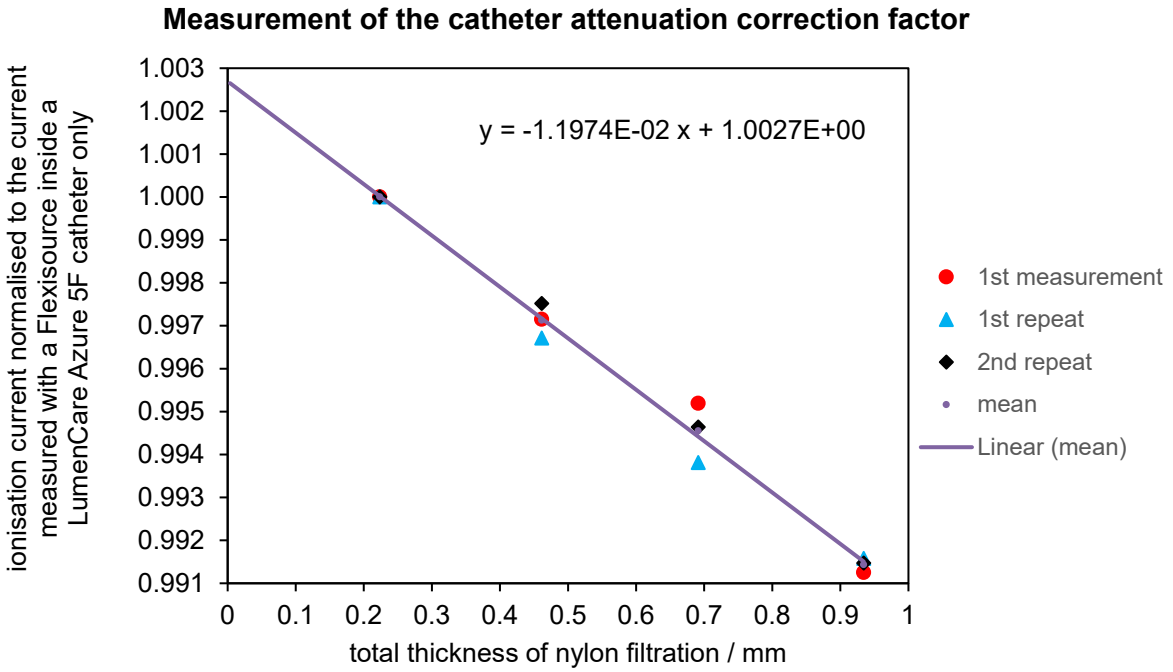


**Figure 11. Ionisation current measured with the RAKR primary standard cavity chamber normalised to the current measured with an HDR $^{192}$Ir Flexisource inside a LumenCare Azure 5F nylon catheter as a function of the total thickness of nylon filtration in the beamline. The catheter attenuation correction factor (1.0027) was determined from the linear fit to all data points.**

The whole measurement procedure from step 1) to 5) was repeated twice. The catheter attenuation correction factor is the y-axis intercept of the linear function that has been fitted to all measurement points shown in Figure 11. Since all measurement points have been normalised to ionisation current measurements with the HDR $^{192}$Ir Flexisource surrounded only by the 5F nylon catheter (y-axis value = 1), the catheter attenuation correction factor, $k_{\text{catheter}}$ = 1.0027, is the y-intercept of the linear function for x = 0 mm.
The standard uncertainty in $k_{\text{catheter}}$ was found through regression analysis of the line fitted to all data points in Figure 11. The intercept was found to be 1.0027 with a relative standard uncertainty of 0.03% and a sensitivity coefficient of -0.003. The gradient was found to be -1.1974E-02 with a relative standard uncertainty of 3.44% and a sensitivity coefficient of 0.003. The combined type A relative standard uncertainty of $k_{\text{catheter}}$ was calculated as $u(k_{\text{catheter}}) = \sqrt{(-0.003 \times 0.03\%)^2 + (0.003 \times 3.44\%)^2} = 0.01\%$. A type B relative standard uncertainty of <0.02% was assigned to $k_{\text{catheter}}$ accounting for a possible ±10% variation in the radial thickness of the 5F catheter due to manufacturing tolerances (conservative estimate), resulting in a total combined relative standard uncertainty of 0.02% in $k_{\text{catheter}}$.

## 4 SUMMARY OF ALL CONVERSION AND CORRECTION FACTORS

**Table 1. Conversion and correction factors for cavity chamber TH100C for HDR $^{192}$Ir RAKR measurements**

| Description | Evaluation method | May 2004 – Apr 2006 )[1] | May 2006 – Feb 2014 )[2] | post-1st May 2006/ pre-1st May 2006 change (%) | Mar 2014 – Jun 2019 )[3] | post-1st Mar 2014/ pre-1st Mar 2014 change (%) | from Jul 2019 )[4] | post-1st Jul 2019/ pre-1st Jul 2019 change (%) |
|---|---|---|---|---|---|---|---|---|
| Density of dry air at 20 °C and 1013.25 mbar (kg m$^{-3}$) | Literature value | 1.2045 | 1.2045 | 0.00 | 1.2045 | 0.00 | 1.2046 | 0.01 |
| Air cavity volume (m$^3$) | Measured | 1.02519E-04 | 1.02519E-04 | 0.00 | 1.02519E-04 | 0.00 | 1.02519E-04 | 0.00 |
| Energy per ion pair, $W_{\text{air}}/e$ (J C$^{-1}$) | Literature value | 33.97 | 33.97 | 0.00 | 33.97 | 0.00 | 33.97 | 0.00 |
| Mass energy absorption coefficient ratio (air to graphite) | MC calculation | 1.0017 | 1.0016 | -0.01 | 1.0016 | 0.00 | 1.0022 | 0.06 |
| Mass stopping power ratio (graphite to air) × fluence perturbation correction factor | MC calculation | 1.0082 | 1.0082 | 0.00 | 1.0082 | 0.00 | 1.0061 | -0.21 |
| Wall correction factor | MC calculation | 1.0442 | 1.0453 | 0.11 | 1.0453 | 0.00 | 1.0417 | -0.34 |
| Central electrode correction factor | MC calculation | 0.9991 | 0.9984 | -0.07 | - | 0.16 | - | - |
| Air gap correction factor | MC calculation | 1.0004 | - | -0.04 | - | - | - | - |
| Point non-uniformity correction factor | MC calculation | 0.9982 | - | 0.18 | - | - | - | - |
| Axial non-uniformity correction factor | MC calculation | - | 0.9981 | -0.19 | 0.9981 | 0.00 | 0.9981 | 0.00 |
| Radial non-uniformity correction factor | MC calculation | - | 1.0000 | 0.00 | 1.0000 | 0.00 | 1.0000 | 0.00 |
| Stem scatter correction factor | Measured | 0.9982 | 0.9983 | 0.01 | 0.9974 | -0.09 | - | 0.26 |
| Polarity correction factor | Measured | 0.9993 | 0.9983 | -0.10 | 0.9995 | 0.12 | 0.9995 | 0.00 |
| Configuration correction factor (= dead volume correction factor) | Finite element modelling | 1.0000 | 1.0000 | 0.00 | 1.0000 | 0.00 | 1.0000 | 0.00 |
| Fraction of energy lost by bremsstrahlung, $(1-\bar{g}_{\text{air}})^{-1}$ | MC calculation | 1.0006 | 1.0007 | 0.01 | 1.0007 | 0.00 | 1.0007 | 0.00 |
| Humidity correction factor | Literature value | 0.9970 | 0.9970 | 0.00 | 0.9970 | 0.00 | 0.9970 | 0.00 |
| Catheter attenuation correction factor | Measured | - | - | - | - | - | 1.0027 | 0.27 |
| Product of all factors above (Gy C$^{-1}$) | Calculated | 2.8802E+05 | 2.8772E+05 | -0.10 | 2.8826E+05 | 0.19 | 2.8834E+05 | 0.03 |
| $k_{\text{ion}}$ (dose rate dependent; typical value for 20 pA) | Measured | 1.0000 | 1.0028 | 0.28 | 1.0028 | 0.00 | 1.0028 | 0.00 |
| $k_{\text{aasc}}$ ($T$ and $p$ dependent, value for STP) | Measured | 1.0160 | 1.0158 | -0.02 | 1.0165 | 0.07 | 1.0165 | 0.00 |

)[1] and )[2] for Nucletron microSelectron-v1 classic HDR $^{192}$Ir source, model designation: 096.001; data from ICRU report 37 (ICRU 1984) used

)[3] for Elekta HDR $^{192}$Ir Flexisource, model designation: 136.147; data from ICRU report 37 (ICRU 1984) used

)[4] for Elekta HDR $^{192}$Ir Flexisource, model designation: 136.147; data from ICRU report 90 (ICRU 2016) used

Table 1 summarises all conversion and correction factors for cavity chamber TH100C. Since the launch of NPL's HDR $^{192}$Ir brachytherapy calibration service in May 2004, the table has been updated on three occasions, in May 2006, March 2014 and July 2019. References to the original files which contain information on the evaluation of all conversion and correction factors mentioned in this report can be found in the notes added to the relevant cells of the HDR $^{192}$Ir brachytherapy primary standard uncertainty analysis spreadsheet (version 3.0, dated 21 August 2023).

Notes on the May 2006 revision:
MC simulations revealed that the air gap correction due to the 0.16 mm wide air gap between the two graphite hemispheres of cavity chamber TH100C was negligible (see Sander and Nutbrown 2006). CPE still applies for measurements of $^{192}$Ir sources, even with the reduced wall thickness of 2 mm behind the air gap along the equator of the graphite sphere. The air gap correction factor was therefore removed from Table 1.
The point non-uniformity correction factor was factorised into two components, an axial and a radial non-uniformity correction factor.
Some of the other MC calculated factors also changed slightly due to the refined MC simulations (see Table 1).
The stem scatter and polarity correction factors, which were originally based on measurements performed with protection level radiation sources, were measured with an HDR $^{192}$Ir source.
The overall change in the measured and MC calculated chamber factors (excluding $k_{\text{ion}}$ and $k_{\text{aasc}}$) was found to be -0.10%.
The dose rate dependent ion recombination correction factor was initially assumed to be 1.0000, based on measurements with protection level sources. However, the Niatel/Boutillon method (Boutillon 1998) was finally adopted to measure $k_{\text{ion}}$ as a function of ionisation current (see Section 3.4.1). For HDR $^{192}$Ir brachytherapy sources with an initial activity of around 370 GBq, ionisation currents of approximately 20 pA are measured with the TH100C primary standard setup, which resulted in $k_{\text{ion}} = 1.0028$.

All other revisions of the conversion and correction factors in March 2014 and July 2019 have been described in this report. The penultimate column in Table 1, labelled 'from Jul 2019', lists the latest set of conversion and correction factors for cavity chamber TH100C. The percentage change of the factors for consecutive revisions is also shown in Table 1 (see columns highlighted in grey).

## 5 UNCERTAINTIES

Tables 2 to 6 summarise the relative standard uncertainties for RAKR measurements with NPL's HDR $^{192}$Ir brachytherapy primary standard chamber TH100C and HDR brachytherapy secondary standard calibrations based on spreadsheet version 3.0 of the uncertainty budget dated 21 August 2023.

**Table 2. Uncertainty components (*k* = 1) contributing to the uncertainty in the primary standard factor**

| Symbol | Quantity, source of uncertainty | Type A (%) | Type B (%) |
|---|---|---|---|
| $(\bar{\mu}_{\text{en}}/\rho)^{\text{air}}_{\text{graphite}}$ | Mass energy absorption coefficient ratio (air to graphite) | - | 0.10 |
| $\bar{S}^{\text{graphite}}_{\text{air}} \cdot k_{\text{fl}}$ | Mass stopping power ratio (graphite to air) × fluence perturbation correction factor | - | 0.08 |
| $k_{\text{wall}}$ | Wall correction factor | - | 0.10 |
| $u_c(\tilde{F})$ | Standard uncertainty | 0.10 | 0.16* |
| $u_c(\tilde{F})$ | Combined standard uncertainty (subtotal) | 0.19 | |
| $k_{\text{an}}$ | Axial non-uniformity correction factor | 0.05 | 0.10 |
| $k_{\text{rn}}$ | Radial non-uniformity correction factor | 0.01 | 0.02 |
| $k_{\text{pol}}$ | Polarity correction factor | 0.02 | - |
| $W_{\text{air}}/e$ | Energy per ion pair (J C$^{-1}$) | - | 0.35** |
| $g$ | Fraction of energy lost by bremsstrahlung | 0.01 | 0.01 |
| $k_{\text{h}}$ | Humidity correction factor | - | 0.05 |
| $\rho_{\text{air}}$ | Density of dry air (kg m$^{-3}$) | - | 0.01 |
| $\rho_{\text{graphite}}$ | Density of high purity graphite (kg m$^{-3}$) | - | 0.04 |
| $V$, Volume of air cavity (cm$^3$) | | | |
| $d_{\text{sphere}}$ | Internal diameter of sphere (mm) | - | 0.09 |
| $V_{\text{insulator}}$ | Volume of protruding insulator (mm$^3$) | - | 0.00*** |
| $V_{\text{gap}}$ | Volume change due to variation in gap width (mm$^3$) | - | 0.02 |
| $u_c(F)$ | Combined standard uncertainty | 0.25 | |

* Type B uncertainties of first three uncertainty components added in quadrature

** Due to correlated uncertainties between the stopping power ratio and $W_{\text{air}}/e$, the uncertainty in $W_{\text{air}}/e$ has been included in the combined uncertainty for the product $\bar{S}^{\text{graphite}}_{\text{air}} \cdot W_{\text{air}}/e \cdot k_{\text{fl}}$.

*** The type B uncertainty is less than 0.005%.

**Table 3. Uncertainty components (*k* = 1) contributing to the uncertainty in the primary standard measurement of air kerma rate**

| Symbol | Quantity, source of uncertainty | Type A (%) | Type B (%) |
|---|---|---|---|
| $F$ | Total primary standard correction | - | 0.25 |
| $k_{\text{elec}}$ | Electrometer charge calibration (nC/'nC') | - | 0.10 |
| $k_{\text{res}}$ | Electrometer resolution (nC) | - | 0.03 |
| $t$ | Time (s) | - | 0.05 |
| $k_{\text{ion}}$ | Ion recombination correction | - | 0.02 |
| $I_{\text{leakage}}$ | Leakage current (A) | 0.05 | - |
| $T$ | Temperature (K) | - | 0.04 |
| $p$ | Pressure (kPa) | - | 0.01 |
| $R_{\text{angular}}$ | Angular response change | - | 0.09 |
| $R$ | Repeatability | 0.10 | - |
| $u_c(\dot{K}_{\text{air}})$ | Combined standard uncertainty | 0.31 | |

**Table 4. Uncertainty components (*k* = 1, unless otherwise specified) contributing to the uncertainty in the measured RAKR of the HDR $^{192}$Ir source**

| Symbol | Quantity, source of uncertainty | Type A (%) | Type B (%) |
|---|---|---|---|
| $\dot{K}_{\text{air}}$ | Air kerma rate | - | 0.31 |
| $k_{\text{aasc}}$ | Air attenuation and scatter correction | 0.02 | - |
| $k_{\text{catheter}}$ | Catheter attenuation correction | 0.01 | 0.02 |
| $k_{\text{dec}}$ , | Decay correction | | |
| $t_{1/2}$ | Half-life of $^{192}$Ir (days) | - | 0.01 |
| $t_{\text{now}}$ | Time of measurement | - | 0.00* |
| $d$, Centre-to-centre source-chamber distance (mm) | | | |
| $d_{\text{pos}}$ | Catheter position | - | 0.03 |
| $d_{\text{source}}$ | Source position in 5F catheter | - | 0.03 |
| $d_{\text{cath-ap}}$ | 5F catheter to back of aperture | - | 0.01 |
| $d_{\text{ap-cham}}$ | Front of aperture to chamber | - | 0.01 |
| $S_{\text{lat}}$ | Lateral source positioning | - | 0.03 |
| $S_{\text{spec}}$ | Source spectrum | - | 0.10 |
| $A$ | Source alignment in catheter | - | 0.01 |
| $u_c(\dot{K}_R)$ | Combined standard uncertainty | 0.33 | |
| $U(\dot{K}_R)$ | Expanded uncertainty (*k* = 2) | 0.66 | |
| $U(\dot{K}_R)$ | **Report value** (expanded uncertainty (*k* = 2), rounded up to nearest 1 dp) | **0.7** | |

* The type B uncertainty is less than 0.005%.

**Table 5. Uncertainty components (*k* = 1, unless otherwise specified) contributing to the uncertainty in the calibration of a well-type chamber**

| Symbol | Quantity, source of uncertainty | Type A (%) | Type B (%) |
|---|---|---|---|
| $\dot{K}_R$ | Reference air kerma rate | - | 0.33 |
| $k_{\text{elec}}$ | Electrometer current calibration (nA/'nA') | - | 0.10 |
| $k_{\text{res}}$ | Electrometer resolution | - | 0.03 |
| $I_{\text{leakage}}$ | Leakage current (A) | 0.06 | - |
| $T$ | Temperature (K) | - | 0.04 |
| $p$ | Pressure (kPa) | - | 0.01 |
| $k_{\text{dec}}$ , | Decay correction | | |
| $t_{1/2}$ | Half-life of $^{192}$Ir (days) | - | 0.01 |
| $t_{\text{now}}$ | Time of measurement | - | 0.00* |
| $k_{\text{ion}}$ | Ion recombination correction | - | 0.03 |
| $S_{\text{p}}$ | Positioning in source holder | - | 0.01 |
| $R$ | Repeatability | 0.05 | - |
| $u_c(N_{\dot{K}_R})$ | Combined standard uncertainty | 0.36 | |
| $U(N_{\dot{K}_R})$ | Expanded uncertainty (*k* = 2) | 0.72 | |
| $U(N_{\dot{K}_R})$ | **Report value** (expanded uncertainty (*k* = 2), rounded up to nearest 1 dp) | **0.8** | |

* The type B uncertainty is less than 0.005%.

**Table 6. Uncertainty components (*k* = 1, unless otherwise specified) contributing to the uncertainty in the calibration of a Farmer chamber mounted on a Nucletron source calibration jig**

| Symbol | Quantity, source of uncertainty | Type A (%) | Type B (%) |
|---|---|---|---|
| $\dot{K}_R$ | Reference air kerma rate | - | 0.33 |
| $k_{\text{elec}}$ | Electrometer charge calibration (nC/'nC') | - | 0.10 |
| $k_{\text{res}}$ | Electrometer resolution | - | 0.03 |
| $t$ | Time (s) | - | 0.05 |
| $I_{\text{leakage}}$ | Leakage current (A) | 0.06 | - |
| $T$ | Temperature (K) | - | 0.04 |
| $p$ | Pressure (kPa) | - | 0.01 |
| $k_{\text{dec}}$ , Decay correction | | | |
| $t_{1/2}$ | Half-life of $^{192}$Ir (days) | - | 0.01 |
| $t_{\text{now}}$ | Time of measurement | - | 0.00* |
| $D$, Source-chamber distance (mm) | | | |
| $d_{\text{sep}}$ | Catheter separation | - | 0.20 |
| $D_{\text{cath1}}$ | Source in 6F catheter 1 | - | 0.32 |
| $D_{\text{cath2}}$ | Source in 6F catheter 2 | - | 0.32 |
| $A$ | Lateral source positioning | - | 0.02 |
| $B$ | Beam uniformity | - | 0.01 |
| $R$ | Repeatability | 0.10 | - |
| $u_c(N_{\dot{K}_R})$ | Combined standard uncertainty | 0.62 | |
| $U(N_{\dot{K}_R})$ | Expanded uncertainty (*k* = 2) | 1.23 | |
| $U(N_{\dot{K}_R})$ | **Report value** (expanded uncertainty (*k* = 2), rounded up to nearest 1 dp) | **1.3** | |

* The type B uncertainty is less than 0.005%.

## 6 ACKNOWLEDGEMENTS

The authors of this report would like to thank Rebecca Nutbrown for carrying out the refined Monte Carlo simulations to derive some of the primary standard conversion and correction factors as part of the adoption of the recommendations of ICRU report 90 (ICRU 2016). This work was funded by the UK Government's Department for Science, Innovation & Technology through the UK's National Measurement System programmes.

## 7 REFERENCES

Alvarez J T, Sander T, de Pooter J A, Allisy-Roberts P J and Kessler C (2014) Comparison BIPM.RI(I)-K8 of high dose rate $^{192}$Ir brachytherapy standards for reference air kerma rate of the NPL and the BIPM. *Metrologia* **51** (1A) 06024

Attix F H (1984) Determination of $A_{ion}$ and $P_{ion}$ in the new AAPM radiotherapy dosimetry protocol. *Med. Phys.* **11** 714-6

Barnard G P, Axton E J and Marsh A R S (1959) A study of cavity ion chambers with megavoltage X-rays. *Phys. Med. Biol*. **3** (4) 366-94

Barnard G P, Marsh A R S and Hitchman D G I (1964) A study of cavity ion chambers with megavoltage X-rays. *Phys. Med. Biol.* **9** (3) 295-319

Berger M J, Coursey J S, Zucker M A and Chang J (2005) ESTAR, PSTAR, and ASTAR: Computer Programs for Calculating Stopping-Power and Range Tables for Electrons, Protons, and Helium Ions (version 1.2.3). [Online] Available: http://physics.nist.gov/Star [version 2.0.1 (July 2017), accessed 21 September 2023]. National Institute of Standards and Technology, Gaithersburg, MD

Bidmead A M, Sander T, Locks S M, Lee C D, Aird E G A, Nutbrown R F and Flynn A (2010) The IPEM code of practice for determination of the reference air kerma rate for HDR $^{192}$Ir brachytherapy sources based on the NPL air kerma standard. *Phys. Med. Biol.* **55** 3145-59

Bielajew A F (1986) Ionisation cavity theory: a formal derivation of perturbation factors for thick-walled ion chambers in photon beams. *Phys. Med. Biol.* **31** 161-70

Bielajew A F (1990) An analytic theory of the point-source non-uniformity correction factor for thick-walled ionisation chambers in photon beams. *Phys. Med. Biol.* **35** 517-38

Borg J, Kawrakow I, Rogers D W O and Seutjens J P (2000) Monte Carlo study of correction factors for Spencer-Attix cavity theory at photon energies at or above 100 keV. *Med. Phys.* **27** 1804-13

Boutillon M (1998) Volume recombination parameter in ionization chambers. *Phys. Med. Biol.* **43** 2061-72

Boutillon M and Perroche A M (1985) Effect of a change of stopping-power values on the W value recommended by ICRU for electrons in dry air. Comité Consultatif pour les Étalons de Mesure des Rayonnements Ionisants (CCEMRI) Section I/85-8, Bureau International des Poids et Mesures (BIPM), Sèvres

Büermann L and Burns D T (2009) Air-kerma cavity standards. *Metrologia* **46** S24-38

Butler D, Haworth A, Sander T and Todd S (2008) Comparison of $^{192}$Ir air kerma calibration coefficients derived at ARPANSA using the interpolation method and at the National Physical Laboratory using a direct measurement. *Australas. Phys. Eng. Sci. Med.* **31** (4) 332-8

DDEP (2004) Decay Data Evaluation Project: CEA/LNHB (France), PTB (Germany), INEEL (USA), KRI (Russia), LBNL (USA), NPL (United Kingdom), CIEMAT (Spain), CNDC (China), NIST (USA), IFIN-HH (Romania). http://www.lnhb.fr/ddep_wg/ (accessed 9 September 2024)

Douysset G, Sander T, Gouriou J and Nutbrown R (2008) Comparison of air kerma standards of LNE–LNHB and NPL for $^{192}$Ir HDR brachytherapy sources: EUROMET project no 814. *Phys. Med. Biol.* **53** N85-97

Duane S, Bielajew A F and Rogers D W O (1989) Use of ICRU-37/NBS collision stopping powers in the EGS4 system. National Research Council of Canada, *NRCC Report* PIRS-0173, Ottawa

Duane S, Nutbrown R F and Shipley D R (2009) Changes to the NPL air kerma standard for $^{137}$Cs and $^{60}$Co. *NPL report* IR 17

ICRU (1984) International Commission on Radiation Units and Measurements: Stopping Powers for Electrons and Positrons. ICRU report 37 (MD, USA: Bethesda)

ICRU (1985) International Commission on Radiation Units and Measurements: Dose and Volume Specification for Reporting Intracavitary Therapy in Gynecology. ICRU report 38 (MD, USA: Bethesda)

ICRU (1997) International Commission on Radiation Units and Measurements: Dose and Volume Specification for Reporting Interstitial Therapy. ICRU report 58 (MD, USA: Bethesda)

ICRU (2004) International Commission on Radiation Units and Measurements: Dosimetry of Beta Rays and Low-Energy Photons for Brachytherapy with Sealed Sources. ICRU report 72 *J. ICRU* **4** (Oxford: Oxford University Press)

ICRU (2016) International Commission on Radiation Units and Measurements: Key data for ionizing-radiation dosimetry: measurement standards and applications. ICRU report 90 *J. ICRU* **14** (Oxford: Oxford University Press)

Kawrakow I (2000a) Accurate condensed history Monte Carlo simulation of electron transport. I. EGSnrc, the new EGS4 version. *Med. Phys.* **27** 485-98

Kawrakow I (2000b) Accurate condensed history Monte Carlo simulation of electron transport. II. Application to ion chamber response simulations. *Med. Phys.* **27** 499-513

Kawrakow I, Mainegra-Hing E, Rogers D W O, Tessier F and Walters B R B (2018a) The EGSnrc Code System: Monte Carlo simulation of electron and photon transport. *Technical Report* PIRS 701, National Research Council of Canada, Ottawa, Canada

Kawrakow I, Mainegra-Hing E, Tessier F, Townson R and Walters B R B (2018b) EGSnrc C++ class library. *Technical Report* PIRS 898, National Research Council of Canada, Ottawa, Canada

Kessler C, Sander T and Maughan D J (2023) Key comparison BIPM.RI(I)-K8 of high dose-rate $^{192}$Ir brachytherapy standards for reference air kerma rate of the NPL and the BIPM. *Metrologia* **60** (1A) 06012

Pearce A (2008) Recommended Nuclear Decay Data. *NPL report* IR 6

Perez-Calatayud J, Ballester F, Das R K, DeWerd L A, Ibbott G S, Meigooni A S, Ouhib Z, Rivard M J, Sloboda R S and Williamson J F (2012) Dose calculation for photon-emitting brachytherapy sources with average energy higher than 50 keV: Full report of the AAPM and ESTRO. Report of the High Energy Brachytherapy Source Dosimetry (HEBD)

Working Group, ISBN: 978-1-936366-17-0, American Association of Physicists in Medicine, MD, USA

Picard A, Davis R S, Gläser M and Fujii K (2008) Revised formula for the density of moist air (CIPM-2007). *Metrologia* **45** 149-55

Rogers D W O, Duane S, Bielajew A F and Nelson W R (1989) Use of ICRU-37/NBS radiative stopping powers in the EGS4 system. National Research Council of Canada, NRCC Report PIRS-0177

Rogers D W O and Ross C K (1988) The role of humidity and other correction factors in the AAPM TG-21 dosimetry protocol. *Med. Phys.* **15** 40-8

Rogers D W O, Walters B R B and Kawrakow I (2018) BEAMnrc Users Manual. Technical Report PIRS-0509, National Research Council of Canada, Ottawa, Canada

Sander T and Nutbrown R F (2006) The NPL air kerma primary standard TH100C for high dose rate $^{192}$Ir brachytherapy sources. *NPL report* DQL-RD 004

Smith B R, DeWerd L A and Culberson W S (2020) On the stability of well-type ionization chamber source strength calibration coefficients. *Med. Phys.* **47** 4491-501

## APPENDICES

### A1: DESCRIPTION OF THE ELEKTA HDR $^{192}$IR FLEXISOURCE

From 2004 to 2013, Nucletron microSelectron-v1 classic HDR $^{192}$Ir sources (model designation: 096.001, manufactured by Mallinckrodt Medical B.V., The Netherlands) were used at NPL. This type of brachytherapy source became obsolete at the end of 2013. Since 2014, Elekta HDR $^{192}$Ir Flexisources (model designation: 136.147, manufactured by Curium Netherlands B.V., The Netherlands (formerly Mallinckrodt Medical B.V., The Netherlands)) have been used instead.
The enclosure of the radioactive $^{192}$Ir core of the Elekta HDR $^{192}$Ir Flexisource (see Figure 12) consists of a cylindrical stainless steel AISI 316L capsule (length: 4.6 mm, radial thickness: 95 µm) which is sealed with a stainless steel AISI 316L plug. The $^{192}$Ir cylinder inside the capsule is 3.5 mm long and has a diameter of 0.6 mm. The steel plug is welded to the steel capsule. The other end of the steel capsule is welded to a flexible steel wire which is fitted to a stepper motor in the Flexitron afterloader.

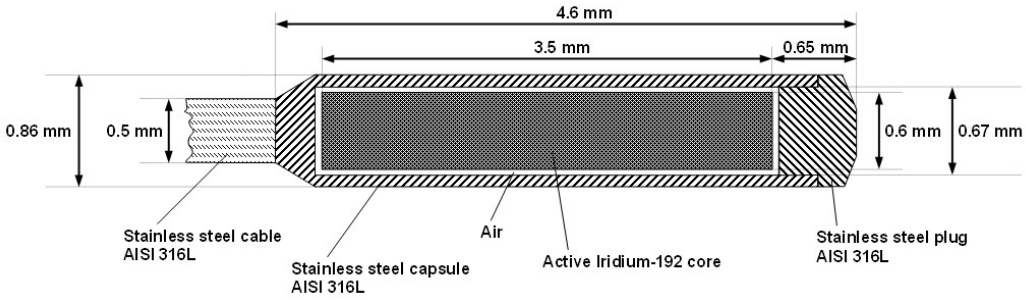


**Figure 12. Cross-sectional view of Elekta HDR $^{192}$Ir Flexisource, model designation: 136.147**

The dimensions shown in Figure 12 are those published by Perez-Calatayud *et al.* (2012), except for the outer diameter of the stainless steel capsule, which was taken from the 'Certificate for Sealed Sources' for HDR $^{192}$Ir Flexisource s/n D85E4717, issued by Curium Netherlands B.V., The Netherlands, dated 17 March 2020. The other dimensions are in good agreement.
The nominal initial activity of the Elekta HDR $^{192}$Ir Flexisource is usually between 370 GBq and 550 GBq.

### A2: BILATERAL AND KEY COMPARISONS

Between 2004 and 2023, NPL's HDR $^{192}$Ir RAKR primary standard was compared against international standards on four occasions.
In 2004, NPL and the Laboratoire National Henri Becquerel (LNHB) in France compared their HDR $^{192}$Ir air kerma standards using four well-type ionisation chambers as transfer instruments (Douysset *et al.* 2008). The results of this bilateral comparison showed the ratios of the reported calibration coefficients, $N_{K,\mathrm{LNHB}}/N_{K,\mathrm{NPL}}$, to be between 1.0047 and 1.0063 which was within the combined relative standard uncertainty of 0.65% reported by both laboratories at the time of the comparison. If the revised conversion and correction factors of NPL's HDR $^{192}$Ir primary standard from 2006 had been used for the LNHB / NPL comparison, the ratios of the calibration coefficients would likely be reduced to between 1.0030 and 1.0046.
In 2007, the combination of a PTW Farmer-type thimble chamber (type 30010) and a Nucletron calibration jig (ref. 077.211) was calibrated for the Peter MacCallum Cancer Centre (Australia) against NPL's HDR $^{192}$Ir primary standard. An air kerma calibration coefficient for the Farmer chamber was also measured at the Australian Radiation Protection and Nuclear

Safety Agency (ARPANSA, Australia). An interpolation method was applied to derive the Farmer chamber's $^{192}$Ir calibration coefficient. A jig scatter correction factor was also measured to enable a comparison with the reference air kerma rate calibration coefficient measured by NPL. The ratio of the reported calibration coefficients, $N_{K,\mathrm{ARPANSA}}/N_{K,\mathrm{NPL}}$, was found to be 1.0017 which was within the combined relative standard uncertainties of 1.2% and 0.6% reported by ARPANSA and NPL, respectively (Butler *et al.* 2008).
In 2010, NPL participated in an indirect comparison of the HDR $^{192}$Ir brachytherapy standards for reference air kerma rate of NPL and the Bureau International des Poids et Mesures (BIPM, France). The comparison result of this BIPM.RI(I)-K8 key comparison was expressed as the ratio of the calibration coefficients for a Farmer chamber (type NE2571) transfer standard, $N_{K,\mathrm{NPL}}/N_{K,\mathrm{BIPM}}$, which was found to be 0.9989 with a combined standard uncertainty of 0.0057 (Alvarez *et al.* 2014). Measurements were performed at NPL with a Nucletron microSelectron-v1 classic HDR $^{192}$Ir source. The primary standard conversion and correction factors were based on data published in ICRU report 37 (ICRU 1984).
In 2022, after the implementation of the recommendations of ICRU report 90 (ICRU 2016), NPL participated in another indirect comparison of the HDR $^{192}$Ir brachytherapy standards for reference air kerma rate of NPL and the BIPM (Kessler *et al.* 2023). Measurements were performed at NPL with an Elekta HDR $^{192}$Ir Flexisource. The comparison result of NPL's second BIPM.RI(I)-K8 key comparison was expressed as the ratio of the calibration coefficients for a well-type ionisation chamber (type Standard Imaging HDR 1000 Plus) transfer standard, $N_{K,\mathrm{NPL}}/N_{K,\mathrm{BIPM}}$, which was found to be 1.0045 with a combined standard uncertainty of 0.0043.

## A3: LONG-TERM STABILITY OF NPL'S HDR $^{192}$IR PRIMARY STANDARD

Since 2002, the long-term stability of NPL's primary standard cavity chamber TH100C has been checked by calibrating three reference ionisation chambers after each HDR $^{192}$Ir source change. Table 7 shows the three reference chambers which are currently in use. The Farmer chamber NE2571A s/n 3272, which was mentioned in NPL Report DQL-RD 004 (Sander and Nutbrown 2006), is no longer being used as a reference chamber due to several catheter breakages of the Nucletron calibration jig over the years, which required several restarts of the calibration histories for the Farmer chamber / jig combination. Since the publication of the IPEM HDR brachytherapy code of practice (Bidmead *et al.* 2010), which recommended well-type ionisation chambers as secondary standards for HDR brachytherapy sources, NPL has only calibrated well chambers but no more thimble chamber / jig combinations for HDR $^{192}$Ir. The Nucletron calibration jig became obsolete in 2013.
The Standard Imaging IVB 1000 well-type chamber shown in Table 7 was introduced as reference ionisation chamber for the HDR $^{192}$Ir primary standard constancy checks in 2010.

**Table 7. Well-type reference chambers for HDR $^{192}$Ir brachytherapy sources used at NPL for primary standard constancy checks**

| Well chamber type | Serial number | Source holder type | Label |
|---|---|---|---|
| Standard Imaging HDR 1000 Plus, part number 90008 | A961699 | Standard Imaging HDR Iridium Source Holder, part number 70010 | SH699 |
| PTW 33004 | 0031 | PTW T33002.1.009 | SH031 |
| Standard Imaging IVB 1000, part number 90009 | H093271 | Standard Imaging HDR Iridium Source Holder, part number 70044 | SH271 |

After each HDR $^{192}$Ir source change at NPL, the RAKR of the new source is measured with the primary standard cavity chamber TH100C. The HDR $^{192}$Ir source is then used to calibrate the three reference ionisation chambers. The well chambers are positioned at least 1 m from any wall and 1 m above floor level on a low scatter surface. At NPL, well-type ionisation chambers are usually operated with a polarising potential of 300 V (collecting electrode positive with respect to earth, i.e. negative current measured).
The $^{192}$Ir source is placed at the dwell position corresponding to the maximum chamber response and the ionisation current is measured at this reference point. For the Standard Imaging well chambers (type HDR 1000 Plus and IVB 1000), a 5 French plastic catheter (nominal outer diameter = 1.7 mm, nominal inner diameter = 1.3 mm) is attached to the brachytherapy treatment unit and pushed to the bottom of the source holder of the well chamber. The black dot on the source holder is aligned with the punch mark on the body of the chamber. For PTW 33004 and PTW 33005 well chambers, a transfer tube is attached to the brachytherapy treatment unit and connected to the top of the source holder of the well chamber.
The well chamber calibration coefficient in terms of Gy C$^{-1}$ at 1 m is the quotient of the primary standard measurement (RAKR in terms of Gy s$^{-1}$ at 1 m) divided by the secondary standard measurement (ionisation current in terms of amps (A)), both decay corrected to the same reference time and date.
The calibration coefficient is obtained with the following equation:

$$N_{\dot{K}_\mathrm{R}} = \frac{\dot{K}_\mathrm{R}(t_\mathrm{ref})}{I(t) \cdot k_\mathrm{ion}(t) \cdot k_\mathrm{dec}(t)} \,, \tag{26}$$

where $\dot{K}_\mathrm{R}(t_\mathrm{ref})$ is the RAKR (Gy s$^{-1}$ at 1 m) of the HDR $^{192}$Ir source at the reference time, $t_\mathrm{ref}$, $I(t)$ is the measured ionisation current in amps (A) at the time of the chamber calibration, obtained with the $^{192}$Ir brachytherapy source positioned inside the well chamber at the dwell position corresponding to maximum chamber response and corrected to standard atmospheric conditions ($T$ = 20 °C, $p$ = 1013.25 mbar and *RH* = 50%), $k_\mathrm{ion}(t)$ is the ion recombination correction factor for the well chamber determined with the HDR $^{192}$Ir source at the time of the chamber calibration and $k_\mathrm{dec}(t)$ is the decay correction factor to the reference time, $t_\mathrm{ref}$. The ion recombination correction factor, $k_\mathrm{ion}$, which is the reciprocal of the charge collection efficiency, $A_\mathrm{ion}$, is measured using a two-voltage technique (Attix 1984), using the following equation for continuous radiation:

$$k_\mathrm{ion} = \left(\frac{4}{3} - \frac{I_{300}}{3 \cdot I_{150}}\right)^{-1} \,, \tag{27}$$

where $I_{300}$ is the ionisation current in A with the polarising voltage set to 300 V and $I_{150}$ is the ionisation current in A with the polarising voltage set to 150 V.
All normalised calibration coefficients for each of the three reference chambers up to April 2023 are shown in Figures 13, 14 and 15. In November 2013, a new calibration history was started when the source type used for HDR brachytherapy calibrations at NPL was changed from Nucletron HDR $^{192}$Ir microSelectron-v1 classic to Elekta HDR $^{192}$Ir Flexisource.
From the measurements carried out until the publication of this report, it can be concluded that variations of the well chamber calibration coefficients of ±0.4% from the running mean can be expected when using the NPL calibration method. If, after an HDR $^{192}$Ir source change, a well chamber calibration coefficient is found to be outside the ±0.4% range from the running mean, this needs to be investigated. The ±0.4% variation of the well chamber calibration coefficients over time is mainly due to variations of the NPL primary standard setups over consecutive years. The long-term stability of the response of the three well chambers was shown to be much tighter, with typical variations of around ±0.15% (see Figure 16). This also confirms the findings of a study on the long-term stability of well-type ionisation chamber source strength calibration coefficients (Smith *et al.* 2020).

In addition to the three reference chambers, three further well-type chambers are calibrated at NPL after each HDR $^{192}$Ir source change with the aim to build up their chamber histories, so that they can potentially replace any of the three reference chambers should they fail in the future.
After each HDR $^{192}$Ir source change at NPL, once it has been confirmed that the long-term stability of the three reference chambers is in the typical range of around ±0.15% and the calibration coefficients for each of the chambers are within ±0.4% of the running mean, the HDR $^{192}$Ir source can be used to calibrate secondary standard well-type ionisation chambers for external customers by applying Equations 26 and 27.

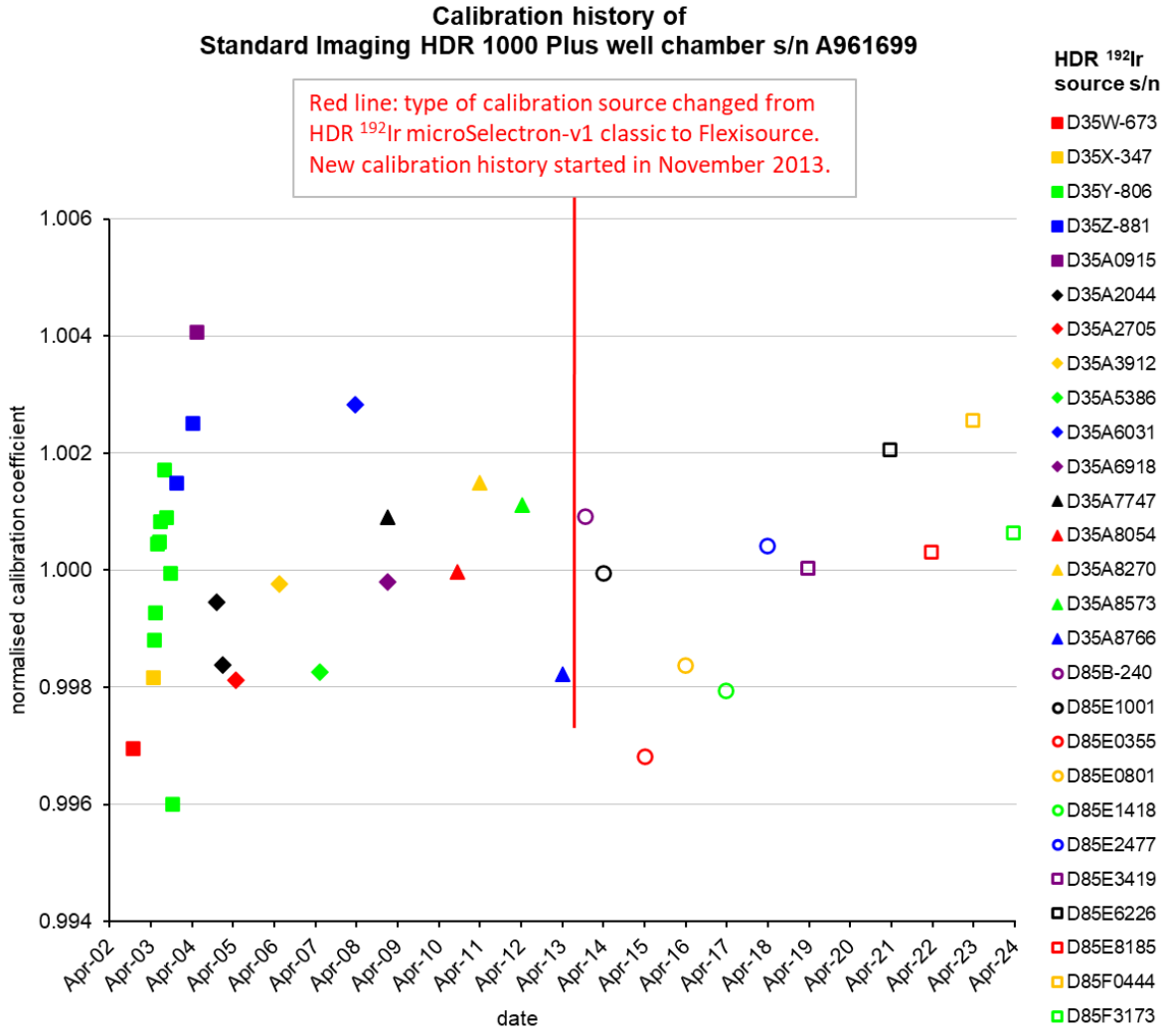


**Figure 13. Calibration coefficients of NPL reference chamber Standard Imaging HDR 1000 Plus (serial number: A961699), normalised to the running mean from November 2002 to April 2013 for measurements with HDR $^{192}$Ir microSelectron-v1 classic sources, and normalised to the running mean from November 2013 to March 2024 for measurements with HDR $^{192}$Ir Flexisources.**
**For consistency, all normalised calibration coefficients for the Flexisource measurements (see data points from November 2013) have been corrected to the latest set of conversion and correction factors, based on both the 2014 and 2019 revisions of the primary standard factors as discussed in this report. The running mean of the RAKR calibration coefficients for $^{192}$Ir measured for this well chamber from November 2013 to March 2024 is 1.284E+2 Gy C$^{-1}$.**

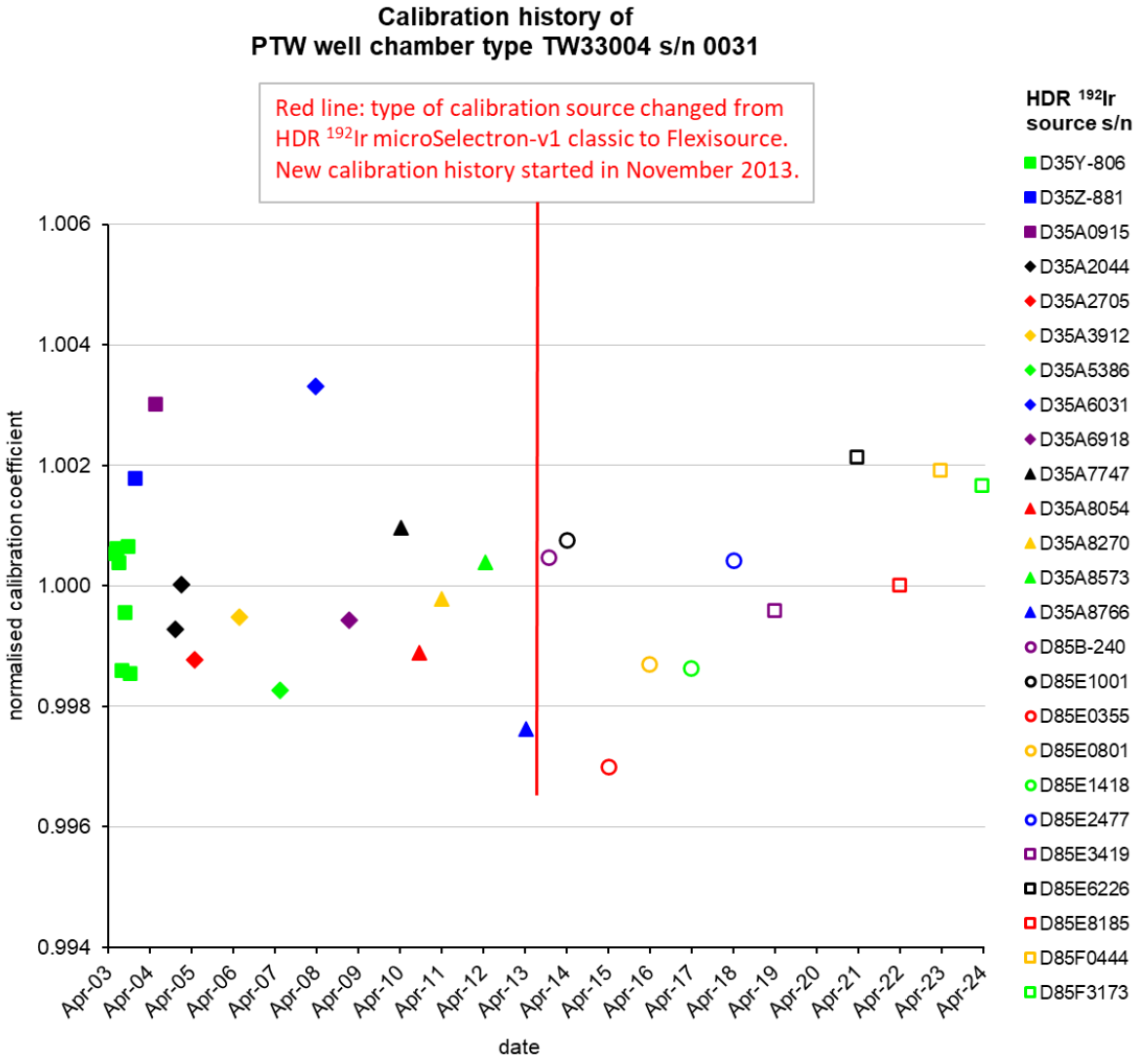


**Figure 14. Calibration coefficients of NPL reference chamber PTW 33004 (serial number: 0031), normalised to the running mean from June 2003 to April 2013 for measurements with HDR $^{192}$Ir microSelectron-v1 classic sources, and normalised to the running mean from November 2013 to March 2024 for measurements with HDR $^{192}$Ir Flexisources.**
**For consistency, all normalised calibration coefficients for the Flexisource measurements (see data points from November 2013) have been corrected to the latest set of conversion and correction factors, based on both the 2014 and 2019 revisions of the primary standard factors as discussed in this report. The running mean of the RAKR calibration coefficients for $^{192}$Ir measured for this well chamber from November 2013 to March 2024 is 2.502E+2 Gy C$^{-1}$.**

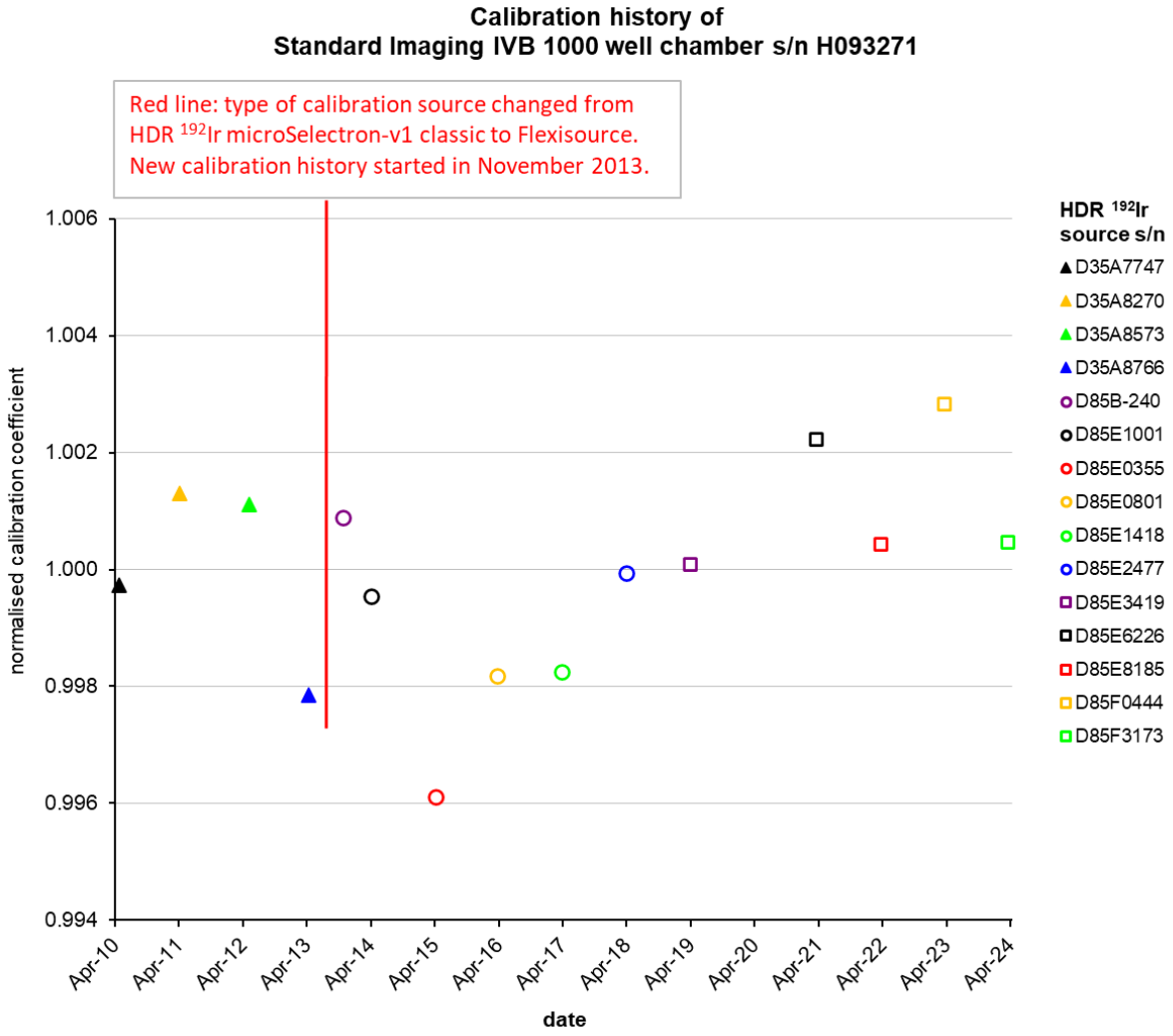


**Figure 15. Calibration coefficients of NPL reference chamber Standard Imaging IVB 1000 (serial number: H093271), normalised to the running mean from May 2010 to April 2013 for measurements with HDR $^{192}$Ir microSelectron-v1 classic sources, and normalised to the running mean from November 2013 to March 2024 for measurements with HDR $^{192}$Ir Flexisources.**
**For consistency, all normalised calibration coefficients for the Flexisource measurements (see data points from November 2013) have been corrected to the latest set of conversion and correction factors, based on both the 2014 and 2019 revisions of the primary standard factors as discussed in this report. The running mean of the RAKR calibration coefficients for $^{192}$Ir measured for this well chamber from November 2013 to March 2024 is 1.229E+2 Gy C$^{-1}$.**

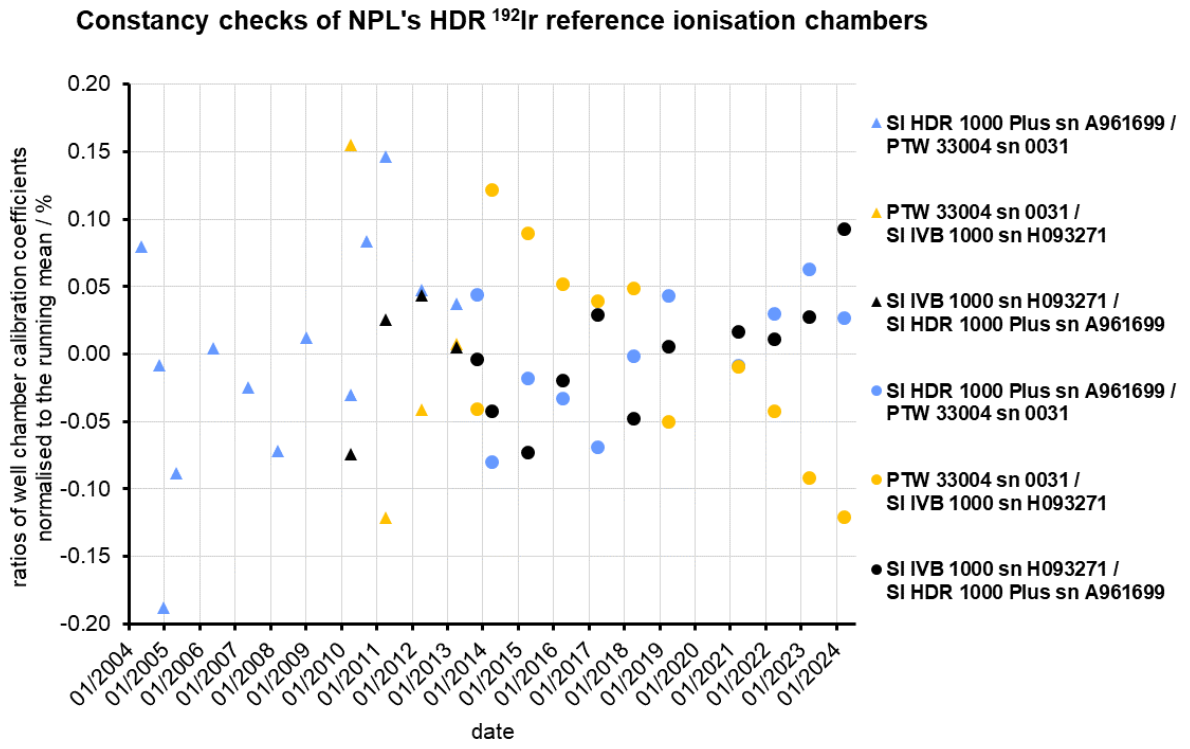


**Figure 16. Ratios of calibration coefficients (normalised to the running mean) for three different well-type chambers which were calibrated with twelve different Nucletron microSelectron-v1 classic HDR $^{192}$Ir sources (see triangular data points) and eleven different Elekta HDR $^{192}$Ir Flexisources (see circular data points). All measurements since the launch of NPL's HDR brachytherapy calibration service in May 2004 are shown. The same HDR $^{192}$Ir source was used to obtain the data points in November 2004 and January 2005. The Standard Imaging IVB 1000 well chamber s/n H093271 was introduced as reference chamber in April 2010, when it replaced the previously used Farmer chamber / Nucletron jig combination. 96% of the ratios of the well chamber calibration coefficients were found to be within ±0.15% of the running mean, which indicates a good long-term stability of all three well chambers.**